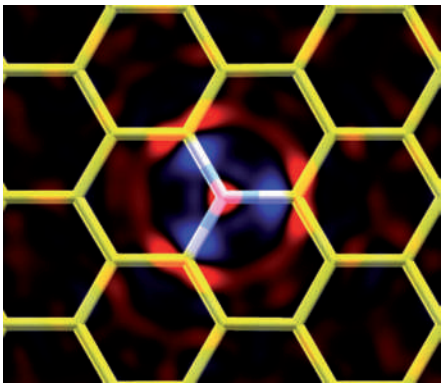

Figure 2 | DFT results for the changes in electron density due to bonding. The blue (red) colour shows a lower (higher) electron density than in the case in which the independent atomic model is used[1].

out the expected contrast difference. As a consequence, the two types of atom cannot be distinguished from each other, on physical grounds. This also shows that first-principle calculations should be used to take advantage of what sophisticated optics has to offer

The other popular concept in HRTEM is that of the 'ideally weak object'. As discussed in textbooks[12], a weak object is realized by a very thin sample consisting of atoms of low nuclear charge, which, owing to their weak electron scattering, induce only very weak phase shifts in the imaging electron-wave field. For such an idealized object, theory[13,14] yields phase-shift contrast that, as long as standard conditions are applied for acquiring an image, provides a direct representation of the scattering potential. This greatly aids image interpretation and has often served as an argument for deriving atomic-structure information from only a single acquisition, thus avoiding the painstaking effort needed to take image series and engage in complicated and time-consuming numerical procedures for electron-wavefunction reconstruction. Now, transmission electron microscopes do not transmit equally well all spatial frequencies that, in a Fourier representation, are required to describe an object structure correctly. For example, the microscope cuts spatial frequencies both in the high- and low-frequency range, thus acting as a low- and high-pass filter. Meyer and colleagues show that in the standard-conditions single acquisition mode, the contrast features induced by charge transfer are suppressed, making the bonding-induced effect unobservable. Yet single-layer graphene is, with respect to electron scattering, the weakest object so far available. Taking image series under defined variable-focus conditions allows expansion of the spatial-frequency characteristics of a microscope. This has to become part of the everyday routine of microscopy on the atomic scale.

To 'see' atoms and to measure the local electronic effect of integrating an atom into a solid is a long-standing dream in materials science. The recent work on graphene is a great step in this direction. In essence this means nothing less than an uncompromising application of quantum mechanics not only to the calculation of the electron structure in solids but also to the treatment of contrast formation in electron optics. ❐

Knut W. Urban is at the Peter Grünberg Institute at the Helmholtz Research Centre Jülich, D-52425 Jülich, Germany. He is also a JARA Senior Professor at RWTH Aachen University.
e-mail: k.urban@fz-juelich.de

References

1. Meyer, J. C. *et al. Nature Mater.* **10,** 209–215 (2011).
2. Meyer, J. C. *et al. Nature* **446,** 60–63 (2007).
3. Urban, K. W. *Nature Mater.* **8,** 260–262 (2009).
4. Jinschek, J. R. *et al. Carbon* **49,** 556–562 (2011).
5. Lim, S. H., Li. R., Ji, W. & Lin, J. *Phys. Rev. B* **76,** 195406 (2007).
6. Wiesendanger, R. (ed.) *Scanning Probe Microscopy: Analytical Methods* (Springer, 1998).
7. Muller, D. A. *et al. Science* **319,** 1073–1076 (2008).
8. Suenaga, K. & Koshino, M. *Nature* **468,** 1088–1090 (2010).
9. Urban, K. W. *Science* **321,** 506–510 (2008).
10. Doyle, P. A. & Turner, P. S. *Acta Cryst. A* **24,** 390–397 (1968).
11. Deng, B. & Marks, L. D. *Acta Cryst. A*, **62,** 208–216 (2006).
12. Williams, D. B. & Carter, C. B. *Transmission Electron Microscopy* 2nd edn (Springer, 2009).
13. Scherzer, O. *J. Appl. Phys.* **20,** 20–29 (1949).
14. Lentzen, M. *Microsc. Microanal.* **12,** 191–205 (2006).

SYNTHETIC VACCINES

Immunity without harm

Multilamellar lipid vesicles with crosslinked walls carrying protein antigens in the vesicle core and immunostimulatory drugs in the vesicle walls generate immune responses comparable to the strongest live vector vaccines.

Abhinav P. Acharya and Niren Murthy

Preventive (prophylactic) vaccines have greatly helped the global eradication of some infectious viral diseases, for example poliomyelitis or smallpox[1]. However, vaccines used against pathogens such as the HIV and the hepatitis C virus (HCV) have for the most part failed. One problem is that vaccines based on attenuated viruses, despite generating protective immunity[2,3], are frequently too toxic for clinical use. On the other hand, non-viral vaccines, which typically have an excellent toxicity profile, are relatively ineffective at promoting immunity. It is therefore necessary to develop a vaccination strategy that can generate effective immunity and have low toxicity. As reported in *Nature Materials*, Irvine and colleagues have achieved an important step in this direction[4]: a non-viral vaccine carrier that provides immune responses comparable to viral vectors[5].

The vaccine carriers are multilamellar vesicles (liposomes) with crosslinked bilayers that entrap protein antigens in the vesicle core, and immunostimulatory Toll-like receptor (TLR) ligands in between bilayers (TLR is a protein that recognizes structural patterns). Irvine and colleagues showed that the crosslinked liposomes act as a controlled-release reservoir of protein antigen and can also target dendritic cells *in vivo*. Dendritic-cell targeting is a key part of the multi-step process by which vaccines activate antigen-specific memory T cells[6] — cells that recognize and rapidly clear pathogens that caused previous infections. In this process (Fig. 1), dendritic cells pick up the injected liposomes and present the delivered antigen and immunostimulatory molecules to cytotoxic T cells. The dendritic cells secrete cytokines — cell-signalling protein molecules — that help activate T cells against the pathogen-specific antigens. These cells then proliferate and circulate through the body, most of them dying off within a few days. However, a small subset of the population of cytotoxic (or killer) T cells survives in the long term (even for decades), giving rise to memory T cells. On

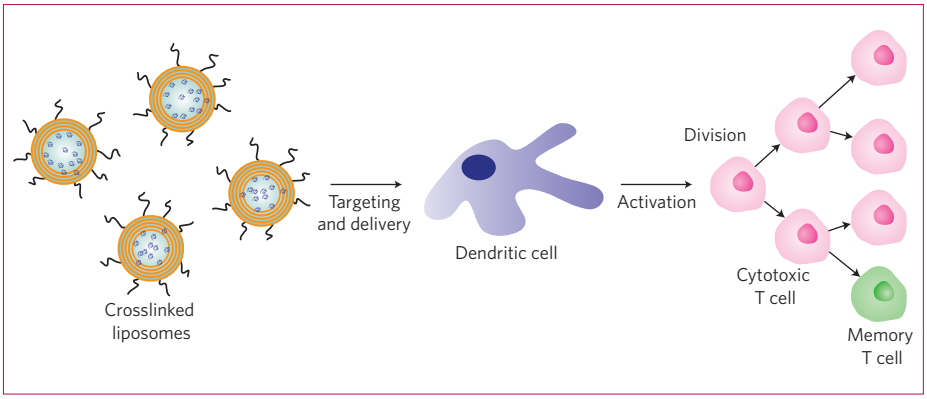

Figure 1 | Crosslinked liposomes target and deliver antigen and immunostimulatory drugs to dendritic cells to trigger the generation of memory T cells. Activated dendritic cells generate cytotoxic T cells, which then divide and clear the infection. Some of the cytotoxic T cells give rise to memory T cells, which survive long term.

infection by a pathogen with the known antigen, the antigen-specific memory T cells proliferate and differentiate into cytotoxic T cells, which clear the infection before it can gain a foothold. Hence, the presence of antigen-specific memory T cells greatly accelerates the timescale and magnitude of the immune response towards the infecting pathogen.

Although the detailed mechanism by which antigen-specific memory T cells are generated is not completely understood, key steps seem to be the presentation of the antigen to T cells, the secretion of cytokines by dendritic cells, and the controlled release of antigen. To secrete the cytokines needed for T cell activation, dendritic cells need to be stimulated by TLR ligands. Thus, several polymeric microparticles have been developed that can deliver both antigen and TLR ligands[7]. However, because these particles have difficulties in reaching the cytosol of dendritic cells, they tend to be less effective as vaccine carriers.

As an alternative, the delivery of vaccines loaded into liposomes is a very attractive strategy not only because the cytosol can be accessed, but also because both antigen and TLR ligands can be easily encapsulated within the same particle, owing to the presence of both aqueous and hydrophobic components. Furthermore, the synthesis of liposomes is simple, it can be performed on a small scale in an aqueous environment, and it provides high encapsulation of proteins. Despite the advantages, however, liposomes have previously not been critically successful as vaccine-delivery vehicles owing to their variable stability and unpredictable release profile[8]. Indeed, liposomes can be destabilized under the shear forces present in biological environments, resulting in structural disintegration and aggregation or fusion, and also have problems with chemical stability because of hydrolysis, oxidation and enzymatic degradation.

Irvine and co-authors avoided the usual problems in the stability and release profile of the liposomes by crosslinking their bilayers with thioether linkages (Fig. 2). Additionally, polyethylene glycol was conjugated on the surface of the resulting interbilayer crosslinked multilamellar vesicles (ICMVs) to enhance their *in vivo* performance. The authors showed that ICMVs have excellent stability in physiological solutions but rapidly break down intracellularly as a result of the presence of lipases — lipid-hydrolysing enzymes — within the cells[4]. They also showed that ICMVs provide both sustained release and intracellular delivery of the entrapped antigen, thus allowing efficient activation of both T and B cells, and the generation of memory T cells. B cells — cells that produce antibodies against antigens — are important because they neutralize pathogens that are circulating in the blood, and it is believed that effective vaccines for pathogens such as HIV will require activation of both T and B cells.

Although ICMVs have shown tremendous potential with the model antigen Ovalbumin, it needs to be seen if this approach shows similar levels of efficacy with protein antigens from pathogens such as HIV and HCV. Also, because the immune system of humans can be substantially different from that of a mouse, determining if ICMVs also have high efficacy in higher animal models is critical. All in all, the concept of crosslinking liposomes with dithiol linkages is a powerful way of delivering protein antigens and TLR ligands to immune cells, with the potential to greatly improve vaccine development and drug delivery. ❐

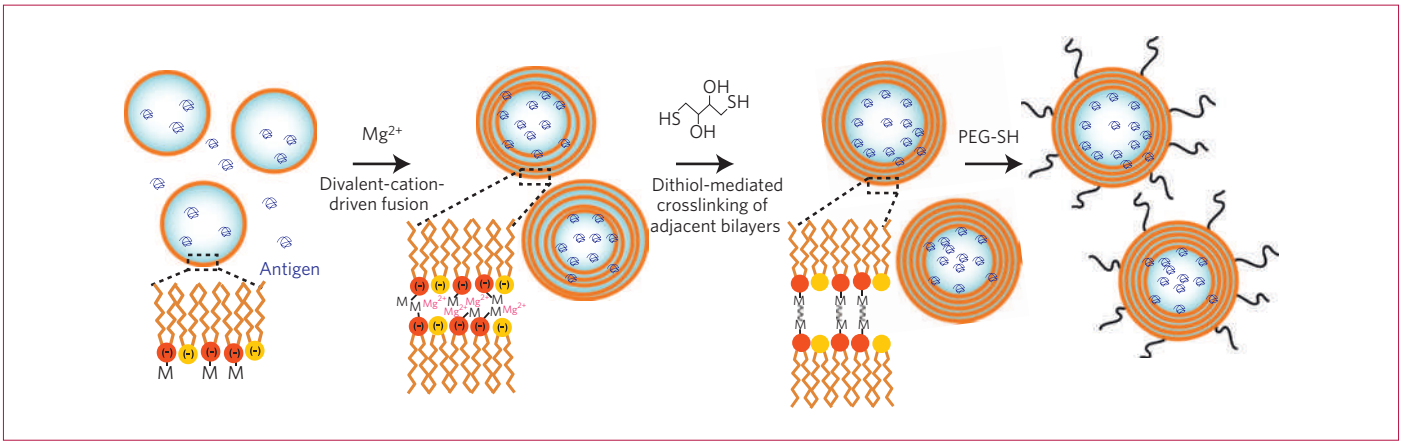

Figure 2 | Interbilayer-crosslinked multilamellar vesicles (ICMVs) encapsulating TLR ligands (not shown) and pathogen-specific antigens were synthesized[4] from dried liposomes by Mg^{2+}-induced fusion and by crosslinking lipid head groups from opposite lipid bilayers with bilayer-permeable dithiols. Thiol-terminated polyethylene glycol (PEG-SH) was then conjugated to the surface of the resulting ICMVs to enhance their performance *in vivo*.

Abhinav P. Acharya and Niren Murthy are at the Department of Biomedical Engineering, Georgia Institute of Technology, 315 Ferst Drive, Atlanta, Georgia 30332, USA.
e-mail: niren.murthy@bme.gatech.edu

References
1. Jacobs, J. F. *et al. Euro Surveill.* **14,** 1–6 (2009).
2. Draper, S. J. & Heeney, J. L. *Nature Rev. Microbiol.* **8,** 62–73 (2010).
3. Ongkudon, C. M., Ho, J. & Danquah, M. K. *Crit. Rev. Biotechnol.* doi:10.3109/07388551.2010.483460 (2010).
4. Moon, J. J. *et al. Nature Mater.* **10,** 243–251 (2011).
5. Zubkova, I. *et al. Vaccine* **27,** 2594–2602 (2009).
6. Lefrancois, L. & Obar, J. J. *Immunol. Rev.* **235,** 206–218 (2010).
7. Johansen, P., Martínez Gómez, J. M. & Gander, B. *Expert Rev Vaccines* **6,** 471–474 (2007).
8. Maurer, N., Fenske, D. B. & Cullis P. R. *Expert Opin. Biol.* **1,** 923–947 (2001).

OXIDE ELECTRONICS

Interface takes charge over Si

The formation of a two-dimensional electron liquid at the interface between two insulating oxides, now extended to oxides on Si, joins a wealth of observations that reveal how electron transfer between layers is responsible for this unusual effect.

Darrell G. Schlom and Jochen Mannhart

Silicon, the backbone of modern electronics, is the most perfected, best understood and most heavily exploited electronic material of the information age we live in. The technological impact of new material systems with functional properties of relevance to semiconductor devices — properties that are not provided by silicon — relies on their successful integration with silicon. Writing in *Nature Communications*, Jae-Wan Park and colleagues report precisely this[1]: the integration of a functional oxide interface on silicon. This oxide system is known to show remarkable properties[1], including a transition from conducting to insulating states that can be reversibly written and erased locally with nanometre precision using techniques based on atomic force microscopy[2]. In addition to its possible role for semiconductor technology, this achievement provides important clues to the origin of the metallic conductivity that can be realized at the interface between these two oxides, $LaAlO_3$ and $SrTiO_3$, which are both insulators.

Whether this effect will have any relevance for silicon electronics depends strongly on whether this is an intrinsic electronic effect, or merely caused by defects. And indeed, this issue has been intensively investigated. Metallic conductivity is observed at the interface between the insulating oxides $LaAlO_3$ and $SrTiO_3$ when thin epitaxial $LaAlO_3$ films are grown on (001)-oriented $SrTiO_3$ single crystals that terminate with a TiO_2 layer[3], as schematically shown in Fig. 1a,b. In contrast, if SrO is the top layer of the $SrTiO_3$ (Fig. 1c), or if amorphous $LaAlO_3$ is grown on TiO_2-terminated $SrTiO_3$ (Fig. 1d), the resulting interfaces are insulating[3,4]. The origin of the interfacial conductivity has been attributed to electronic reconstruction[5], a process in which, owing to electron transfer, some of the Ti^{4+} in the TiO_2 layer at the interface with the $LaAlO_3$ is reduced to Ti^{3+}. In essence, when growing a (001)-oriented $LaAlO_3$ film on TiO_2-terminated $SrTiO_3$, an electrostatic voltage is built up because $LaAlO_3$ consists of charged, alternating planes of LaO^+ and AlO_2^- (ref. 5). The voltage grows with the thickness of the $LaAlO_3$ film to such large values that eventually electrons move from the surface of the $LaAlO_3$ film to the $LaAlO_3$/$SrTiO_3$ interface to occupy Ti 3*d* states there. These 3*d* states form two-dimensional electronic bands that extend parallel to the interface, and thereby provide interfacial

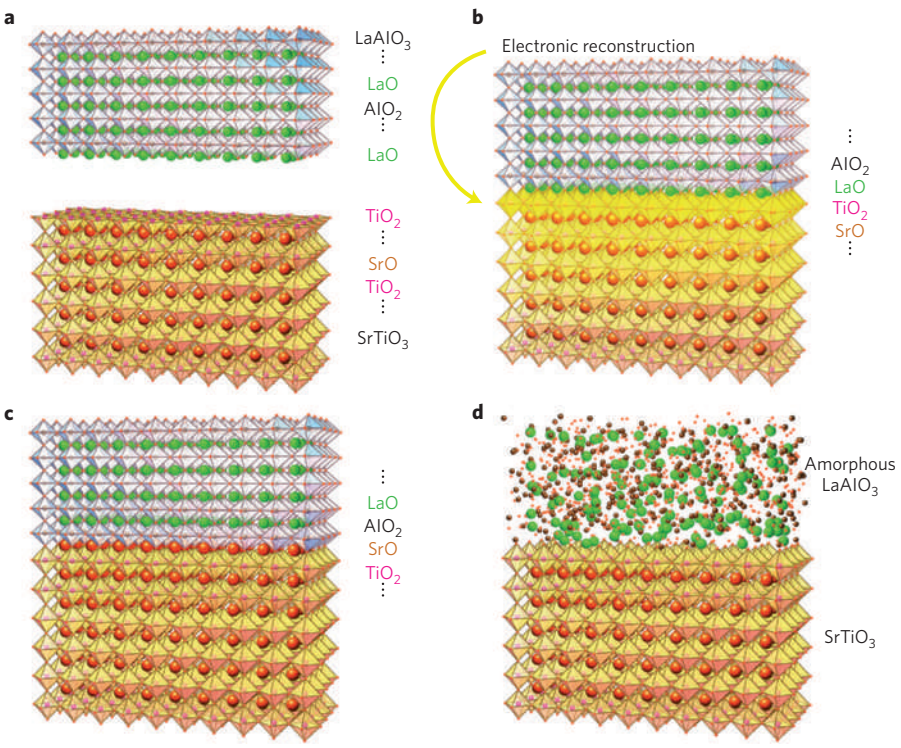

Figure 1 | Subtle differences between $LaAlO_3$/$SrTiO_3$ interfaces result in just one type of interface exhibiting interfacial conductivity. **a**, Schematic of a TiO_2-terminated (001) $SrTiO_3$ single crystal before contact with an epitaxial $LaAlO_3$ overlayer. **b**, Epitaxial $LaAlO_3$ on TiO_2-terminated $SrTiO_3$ is the only interface to exhibit interfacial conductivity, provided it is more than three unit cells thick. **c**, Epitaxial $LaAlO_3$ on SrO-terminated $SrTiO_3$ does not exhibit interfacial conductivity. **d**, Amorphous $LaAlO_3$ on TiO_2-terminated $SrTiO_3$ is also insulating. The interfaces shown are schematic and do not include atom rearrangements including octahedral rotations or the buckling of atomic planes.

Cross-linked multilammelar vesicles

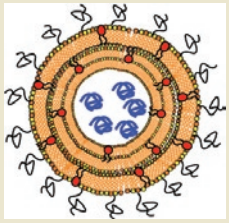

Subunit vaccines seldom activate the potent T-cell responses needed to counteract many viral diseases and cancers because of inefficient presentation of antigens to naive CD8$^+$ T cells. Success to date in encapsulating antigens and adjuvants within unilamellar and multilamellar lipid vesicles is thought to arise from an enhancement of antigen stability and the mimicking of cues normally associated with a protective immune response. Moon *et al.* build on these efforts by covalently crosslinking the concentric membrane bilayers that encapsulate a core filled with model antigen ovalbumin (blue in picture) and embedding the lipid-like Toll-like receptor 4 (TLR4) agonist monophosphoryl lipid A (MPLA; red in picture) within the bilayers. Comparisons with simple liposomes and multilamellar liposomes of the same lipid composition reveal that the new polyethylene glycol–decorated, interbilayer–crosslinked multilamellar vesicles (ICMVs) elicit T-cell and antibody responses to the model antigen ovalbumin in mice comparable to those for strong, live-vector vaccines. Stapling of the bilayers appears to prolong persistence of the vaccine in the serum while optimizing vaccine delivery to antigen-presenting cells. It remains to be seen whether these promising effects will translate to better protective immunity in disease models. (*Nat. Mater.* **10**, 243–251, 2011) *PH*

Immunity through IL-17

Pediatric *Streptococcus pneumoniae* infections represent a significant health problem, despite the existence of effective vaccines. Vaccines cover only a fraction of the extant serotypes, and the population of *S. pneumoniae* colonizing the nasal mucosa is dynamic, necessitating the production of new vaccines. Moffitt *et al.* use a genomic approach to design serotype-independent vaccines that trigger immune responses in mouse models and in human cells. Based on prior work showing that mucosal-derived immunity in adults resistant to *S. pneumoniae* is mediated by IL-17–secreting CD4$^+$ T cells, the researchers first screened a library of pneumococcal proteins for those that stimulate IL-17 secretion *in vitro*. They identified 17 proteins that were present in all 22 of the sequenced *S. pneumoniae* genomes and did not cross-react with human or other bacterial proteins. From those, five that were expressed at high levels in *Escherichia coli* were selected for further testing. Two selected proteins (both components of transport systems) stimulated mouse splenocytes and human peripheral blood monocytes to secrete IL-17. In addition, mice immunized intranasally with those antigens were protected from infection with clinical strains of *S. pneumoniae*; this protection was abrogated by depleting the animals of CD4$^+$ T cells or by inhibiting the IL-17 pathway. The work identifies a new route to immunity as well as a novel set of antigens—none of the antigens overlaps with those that elicit antibody responses. In addition, this approach may be applicable to other mucosal pathogens, of which several exist in humans. (*Cell Host Microbe* **9**, 158–165, 2011) *LD*

RNAi phenotyping in trypanosomes

Although the genome of *Trypanosoma brucei,* the parasite that causes African sleeping sickness, has been sequenced, <10% of the ~7,500 protein-coding genes have been studied systematically by genetic disruption. Alsford *et al.* describe an RNA interference (RNAi)-based, genome-scale approach to phenotyping genes. Using their method, thousands of genes—many previously unannotated—are identified as essential for normal growth in one or more stages of the parasite lifecycle. The approach relies on first creating a library of *T. brucei* cells in which the expression of different regions of the genome are suppressed by an RNAi cassette. In contrast to previous approaches requiring one-by-one construction of vectors that target specific genes, the cassettes express double-stranded RNA transcribed from random fragments of genomic DNA, enabling targeting of >99% of all protein-coding sequences in the genome. Once the cells are grown under conditions of interest, next-generation sequencing is used to identify cassettes containing genes whose knockdown causes cells to grow slowly or not at all. Genes required for parasite growth in conditions that model a human host are potential drug targets. (*Genome Res.* published online, doi:10.1101/gr.115089.110, 1 March 2011) *CM*

Antimalarial fungal pesticide

Entomopathogenic fungi like *Metarhizium anisopliae* have been proposed as promising alternatives to chemical pesticides for controlling a range of insect pests. An issue with using unmodified *M. anisopliae* to control malaria is that it takes as long for the fungus to kill mosquitoes as the time needed for the malarial parasite to complete its life cycle. Therefore, unless the fungus infects the mosquito at the beginning of the parasite life cycle, the mosquito can still spread malaria before it dies. Strategies to accelerate the killing process have been reported (*Nat. Biotechnol.* **25**, 1455–1456, 2007). However, these strategies would likely select for fungal resistance if most mosquitoes are killed before they reproduce. Fang *et al.* address this challenge by engineering *M. anisopliae* to express proteins that block development of the malarial parasite within mosquitoes. Expression of a fusion protein results in 98% clearance of parasites from infected insects, while eliminating the requirement that fungal and parasite infection coincide. Containing the host range of widely disseminated *M. anisopliae* spores remains a potential obstacle to implementation of this biocontrol strategy. Gao *et al.* recently presented a comparative genomic analysis of *M. anisoplae* and *Metarhizium acridum,* a relative with a more restrictive host range. The insights from such approaches may be invaluable in efforts to refine the approach. (*Science* **331**, 1074–1077, 2011; *PLoS Genet.* **7**, e1001264, 2011) *PH*

Mutational load in iPSCs

Safety is a preeminent requirement in any clinical application of induced pluripotent stem cells (iPSCs). Two new studies of the genetic stability of iPSCs may raise some cause for concern. Gore *et al.* sequenced most of the protein-coding regions of 22 human iPSC lines and searched for point mutations, small insertions and deletions, and alternative splicing variants. Each exome had on average six mutations, about half of which were not detected in the progenitor fibroblast lines and must therefore have arisen during cell culture or the reprogramming process itself. In the second study, Hussein *et al.* analyzed copy number variations in 22 human iPSC lines, their progenitor fibroblasts and 17 human embryonic stem cell lines. Early-passage iPSCs had substantially more mutations than late-passage iPSCs or the control cell types, although these mutations did not seem to provide a selective advantage and largely disappeared with passaging. More research is needed to understand the mechanisms underlying the mutational load in iPSCs and their implications for the safety of iPSC-based therapies. (*Nature* **471**, 63–67; 58–62, 2011). *KA*

Written by Kathy Aschheim, Laura DeFrancesco, Peter Hare & Craig Mak

nature materials

ARTICLES

PUBLISHED ONLINE: 20 FEBRUARY 2011 | DOI: 10.1038/NMAT2960

Interbilayer-crosslinked multilamellar vesicles as synthetic vaccines for potent humoral and cellular immune responses

James J. Moon[1,2], Heikyung Suh[1,2,3], Anna Bershteyn[1], Matthias T. Stephan[1,2], Haipeng Liu[1,2], Bonnie Huang[2], Mashaal Sohail[2], Samantha Luo[1], Soong Ho Um[1,2], Htet Khant[4], Jessica T. Goodwin[4], Jenelyn Ramos[4], Wah Chiu[4] and Darrell J. Irvine[1,2,3,5,6]★

Vaccines based on recombinant proteins avoid the toxicity and antivector immunity associated with live vaccine (for example, viral) vectors, but their immunogenicity is poor, particularly for CD8$^+$ T-cell responses. Synthetic particles carrying antigens and adjuvant molecules have been developed to enhance subunit vaccines, but in general these materials have failed to elicit CD8$^+$ T-cell responses comparable to those for live vectors in preclinical animal models. Here, we describe interbilayer-crosslinked multilamellar vesicles formed by crosslinking headgroups of adjacent lipid bilayers within multilamellar vesicles. Interbilayer-crosslinked vesicles stably entrapped protein antigens in the vesicle core and lipid-based immunostimulatory molecules in the vesicle walls under extracellular conditions, but exhibited rapid release in the presence of endolysosomal lipases. We found that these antigen/adjuvant-carrying vesicles form an extremely potent whole-protein vaccine, eliciting endogenous T-cell and antibody responses comparable to those for the strongest vaccine vectors. These materials should enable a range of subunit vaccines and provide new possibilities for therapeutic protein delivery.

Currently licensed vaccine adjuvants (for example, aluminium hydroxide and the oil-in-water emulsion MF59) promote immunity by primarily eliciting humoral immune responses without stimulating cellular immunity[1,2]. As strong CD8$^+$ T cell (CD8T) responses may be required for vaccines against cancer or intracellular pathogens such as human immunodeficiency virus, malaria and hepatitis C, there is great interest in technologies to promote concerted humoral and cellular immune responses[3,4]. To this end, engineered live vaccine vectors such as non-replicating recombinant viruses have been developed[5–7], which can induce both robust antibody responses and massive expansion of functional antigen-specific CD8Ts in murine models. However, safety concerns with live vectors and antivector immunity can complicate development of live vector vaccines[7]. Pre-existing vector-specific immune responses have reduced the immunogenicity of live vector-based vaccines in clinical trials[8], and the immune response raised against live vectors following a priming immunization can render booster immunizations using the same vector problematic[7].

In contrast, non-living synthetic vaccines delivering defined antigens can be rationally designed to avoid antivector immunity[9]. Such 'subunit' vaccines are composed of one or a few selected recombinant proteins or polysaccharides normally present in the structure of the target pathogen. However, subunit vaccines elicit poor or non-existent CD8T responses, owing to the low efficiency of cross-presentation (the uptake and processing of extracellular antigen by immune cells for presentation on class I major histocompatibility complex molecules to naïve CD8Ts)[10]. To promote cross-presentation, synthetic particles loaded with protein antigens and defined immunostimulatory molecules have been used[11–17], mimicking in a reductionist fashion the cues provided to the immune system during infection by pathogens. Liposomes are particularly attractive materials for this application, owing to their low toxicity and immunogenicity, track record of safety in clinical use, ease of preparation, and proven manufacturability at commercial scales[18,19]. Lipid vesicles in the form of unilamellar, multilamellar or polymerized vesicles have been tested as vaccine-delivery materials, with some success[19–23]. Antigens entrapped in lipid vesicles are cross-presented *in vivo*[19,24,25], and liposomal protein vaccines have been shown to elicit protective T-cell-mediated antimicrobial and antitumour immune responses in small-animal models[23,26,27]. However, for diseases such as human immunodeficiency virus and cancer, it is currently believed that extremely potent T-cell responses (in concert with humoral immunity) will be required to control the virus/tumours, and therefore more potent T-cell vaccines are still sought[3,4].

A potential factor influencing the potency of lipid vesicles in vaccine delivery is their limited stability in the presence of serum components. For liposomal cargos that can be processed at high temperature or loaded by diffusion through preformed vesicle membranes, enhanced vesicle stability can be achieved by using high-melting-temperature lipids, especially when combined with cholesterol and/or PEGylation[28]. Uni- and multilamellar vesicles have also been stabilized by polymerizing reactive headgroups at the surface of bilayers[29], polymerizing reactive groups in phospholipid

[1]Department of Materials Science and Engineering, Massachusetts Institute of Technology (MIT), Cambridge, Massachusetts, 02139, USA, [2]Department of Biological Engineering, MIT, Cambridge, Massachusetts, 02139, USA, [3]Howard Hughes Medical Institute, Chevy Chase, Maryland, 20815, USA, [4]National Center for Macromolecular Imaging, Verna and Marrs McLean Department of Biochemistry and Molecular Biology, Baylor College of Medicine, Houston, Texas, 77030, USA, [5]Koch Institute for Integrative Cancer Research, MIT, Cambridge, Massachusetts, 02139, USA, [6]Ragon Institute of MGH, MIT, and Harvard, Boston, Massachusetts, 02129, USA. *e-mail: djirvine@mit.edu.

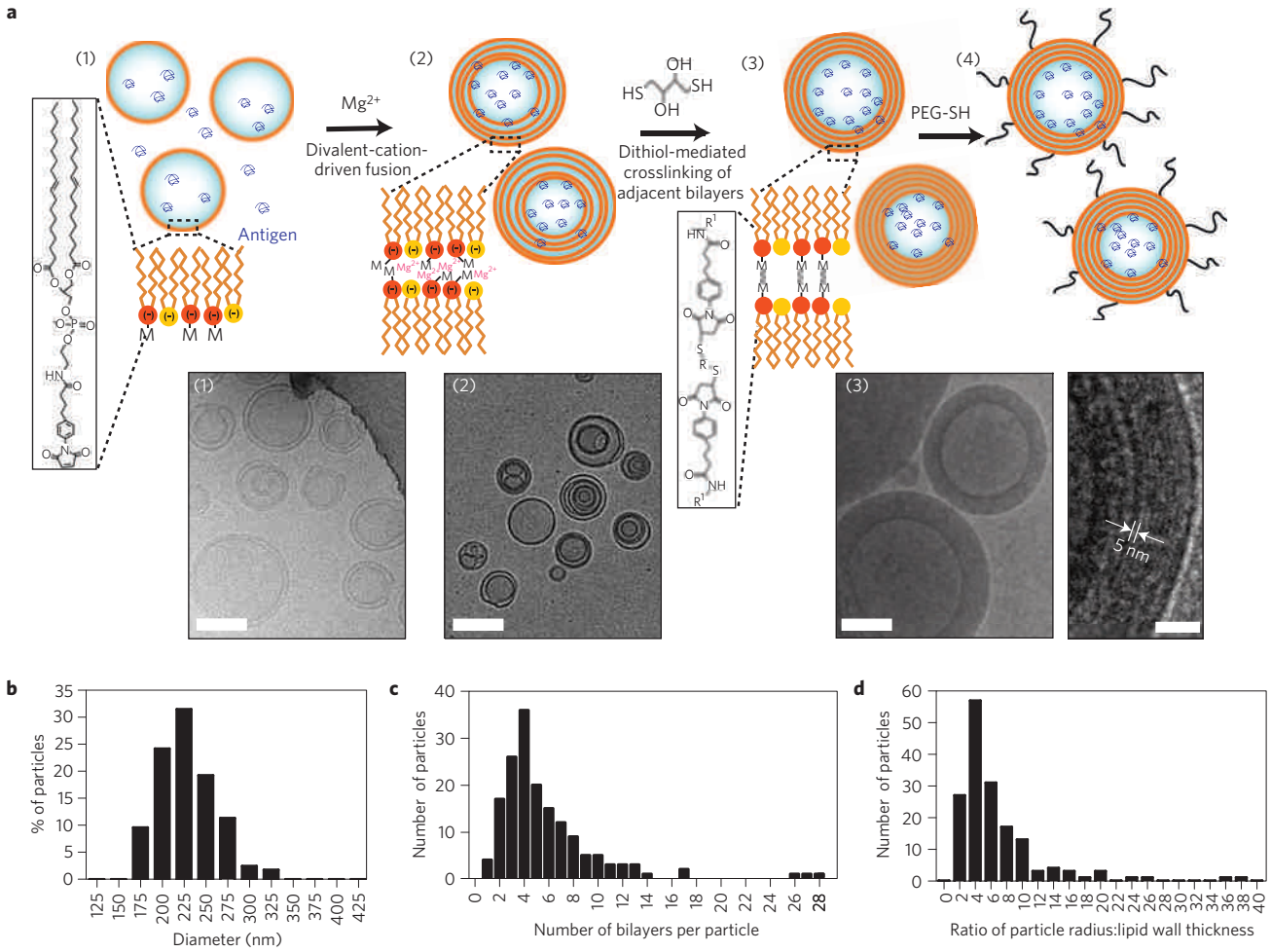

Figure 1 | Synthesis of ICMVs. a, Schematic illustration of ICMV synthesis and cryo-electron-microscope images: (1) anionic, maleimide-functionalized liposomes are prepared from dried lipid films, (2) divalent cations are added to induce fusion of liposomes and the formation of MLVs, (3) membrane-permeable dithiols are added, which crosslink maleimide lipids on apposed lipid bilayers in the vesicle walls, and (4) the resulting lipid particles are PEGylated with thiol-terminated PEG. Cryo-electron-microscope images from each step of the synthesis show (1) initial liposomes, (2) MLVs and (3) ICMVs with thick lipid walls. Scale bars = 100 nm. The right-hand image of (3) shows a zoomed image of an ICMV wall, where stacked bilayers are resolved as electron-dense striations; scale bar = 20 nm. **b**, ICMV particle-size histogram measured by dynamic light scattering. **c**,**d**, Histograms of ICMV properties from cryo-electron-microscope images show the number of lipid bilayers per particle (**c**) and the ratio of particle radius to lipid wall thickness (**d**). ($n = 165$ particles analysed.)

acyl tails[20,29] or polymerizing hydrophobic monomers adsorbed into the hydrophobic interior of membranes[30]. Common to each of these approaches is the concept of polymerizing components in the plane of the bilayer. However, finding polymerization chemistries that can be carried out in mild conditions compatible with vaccine antigens is challenging[20].

Here we describe a new class of lipid drug carriers, interbilayer-crosslinked multilamellar vesicles (ICMVs), formed by stabilizing multilamellar vesicles with short covalent crosslinks linking lipid headgroups across the opposing faces of adjacent tightly stacked bilayers within the vesicle walls. ICMVs encapsulated and stably retained high levels of proteins, releasing entrapped cargo very slowly when exposed to serum (over 30 days) compared with simple liposomes or multilamellar vesicles (MLVs) of the same lipid composition. However, these vesicles were quickly degraded in the presence of lipases normally found at high levels within intracellular compartments[31]. Using this new vesicle structure to co-entrap high levels of a model protein antigen (ovalbumin, OVA) and a lipid-like immunostimulatory ligand (monophosphoryl lipid A, MPLA), we carried out immunization studies in mice and found that ICMVs elicited robust antibody titres ~1,000 times greater than simple liposomes and ~10 times greater than MLVs of identical lipid compositions. Unlike live vectors, which are often only effective for a single injection administered to a vector-naïve individual[7], these synthetic vesicles triggered steadily increasing humoral and CD8T responses following repeated administrations, with antigen-specific T cells expanding to a peak of nearly 30% of the total CD8Ts in blood following a prime and two booster immunizations. These new materials may thus open the door to subunit vaccines that are both safe and highly effective for generating both humoral and cellular immunity.

We introduced covalent crosslinks between functionalized lipid headgroups of adjacent, apposed bilayers within preformed MLVs to form ICMVs (Fig. 1a): in a typical synthesis, dried phospholipid films containing 1,2-dioleoyl-*sn*-glycero-3-phosphocholine (DOPC), anionic 1,2-di-(9Z-octadecenoyl)-sn-glycero-3-phospho-(1'-rac-glycerol) (DOPG) and the anionic maleimide-headgroup lipid 1,2-dioleoyl-*sn*-glycero-3-phosphoethanolamine-*N*-[4-(p-maleimidophenyl) butyramide (MPB) in a 4:1:5 molar ratio were hydrated and sonicated to form simple liposomes (step (1)). Divalent cations (for example, Mg^{2+}) were added to the liposomes to induce vesicle fusion and the

Table 1 | Particle characterization at each step of ICMV synthesis.

Synthesis step (Fig. 1a)	1	2	3	4
Samples	Liposomes	Mg^{2+}-fused MLVs	ICMVs	PEGylated ICMVs
Hydrodynamic diameter* (nm)	192±39	220±26	244±17	263±20
Polydispersity index	0.385±0.11	0.217±0.053	0.223±0.11	0.183±0.025
Zeta potential (mV)	−0.141±0.44	−0.151±0.67	−0.415±0.33	−2.34±0.44
Diameter after 7 days at 4 °C (nm)	N/A	N/A	1,610±570	265±27
Diameter after lyophilization (nm)	N/A	N/A	N/A	2,960±1,800
Diameter after lyophilization with 3% sucrose (nm)	N/A	N/A	N/A	269±41
Fraction of lipid surface exposed†	0.37±0.023	0.15±0.025	0.19±0.010	N/A

*Measured by dynamic light scattering. †The fraction of lipid exposed on the external surface of vesicles decreased after interbilayer crosslinking as measured by a lamellarity assay[36]. All values given as mean±s.d.

formation of MLVs as reported previously[32] (step (2)). To introduce crosslinks between adjacent bilayers in the MLVs, dithiothreitol (DTT) was then added to the vesicle suspension to act as a membrane-permeable crosslinker, forming a covalent linkage between maleimide headgroups of apposed membranes brought into proximity by the cation salt bridges formed between vesicle layers (step (3)). PEGylation is a well-known strategy to increase the serum stability and blood circulation half-life of lipid vesicles[18]. Thus, as a final step, the vesicles were washed and residual maleimide groups exposed on the external surfaces of the particles were capped with thiol-terminated polyethylene glycol (PEG) (step (4)).

The diameter/polydispersity of the particles will determine the cell types capable of internalizing these particles[33], whereas the number of bilayers comprising the vesicle walls would be expected to impact the stability of the vesicles and their ability to retain/slowly release cargos in the presence of serum. To evaluate these properties and better understand the process of ICMV formation, we characterized the products at each step of the synthesis. The initial liposomes formed by sonication (step (1)) had hydrodynamic diameters of ∼190 nm, and the size increased slightly to ∼240 nm following Mg^{2+}-mediated vesicle fusion (step (2)) and subsequent DTT 'stapling' of the bilayers (step (3), Table 1). The resulting ICMVs showed a unimodal, relatively narrow size distribution (comparable to that of common lipid-vesicle or polymer-nanoparticle preparations[12,21]), and there was no evidence for gross aggregation of particles during the crosslinking step from dynamic light scattering or cryo-electron microscopy (Fig. 1a,b, and Table 1). Addition of thiol-terminated PEG to DTT-treated vesicles quenched remaining detectable maleimide groups on the surfaces of MLVs and introduced PEG chains on ∼2 mol% of the surface-exposed lipids of ICMVs without significantly altering particle diameters (Supplementary Fig. S1a,b and Table 1). PEGylated ICMVs stored at 4 °C or 37 °C in PBS remained stable over 7 days, and they were amenable to lyophilization with 3% sucrose added as an excipient[34], highlighting their compatibility with long-term storage conditions (Table 1 and data not shown). We imaged the initial liposomes, Mg^{2+}-fused MLVs and final ICMVs by cryo-electron microscopy (Fig. 1a), and saw that crosslinking with DTT led to the formation of vesicles with thick multilamellar walls composed of tightly stacked bilayers resolved as ∼4–5 nm electron-dense striations. The median number of bilayers per particle was 4.4 (interquartile range 3.3–6.9), and the median particle-radius-to-lipid-wall-thickness ratio was 3.8 (interquartile range 2.4–6.8; Fig. 1c,d). Interestingly, the majority of ICMVs had vesicle walls composed of concentric bilayers, although a few examples of ICMVs with surface defects in the form of incomplete external lipid layers could also be found (Supplementary Fig. S2). Consistent with the increased lamellarity of the vesicles following cation-mediated fusion and DTT crosslinking observed by electron microscopy imaging, the fraction of lipids exposed on the external surfaces of the vesicles decreased in steps (2) and (3) of the synthesis, as measured by a bulk dye-quenching lamellarity assay[35] (Table 1). Chemical evidence for crosslinking between the maleimide lipids following DTT treatment was found in thin-layer chromatography and matrix-assisted laser desorption/ionization time-of-flight measurements on ICMVs (Supplementary Fig. S3 and data not shown). Importantly, both the particle size and individual lamellarity distributions were unimodal, with less than 3% contaminating unilamellar vesicles and no large aggregates, which could skew the functional properties (for example, protein release) of the particles. The ICMVs have a size that should be avidly taken up by monocytes and dendritic cells[36], and a crosslinked multilamellar wall structure that will stabilize protein entrapment compared with traditional unilamellar or multilamellar liposomes.

Analysis of the conditions required to form stable vesicles provided insight into the mechanisms of ICMV formation. Following interbilayer crosslinking, ICMVs could be collected by centrifuging at 14,000 *g* for 4 min ('low-speed conditions'), whereas simple liposomes or MLVs of identical lipid composition required ultracentrifugation to pellet. Using the mass of particles collected by low-speed centrifugation as a surrogate measure of crosslinked vesicle yield, we found that both divalent-cation-mediated fusion (Fig. 1a step (2), either Mg^{2+} or Ca^{2+}) and DTT treatment (step (3)) were required for ICMV formation (Table 2; entries 1–3). Precursor vesicles treated with either Mg^{2+} or DTT alone even at ×10 molar excess relative to maleimide groups did not generate significant yields of particles (Table 2, entries 4–6). In addition, at least 25 mol% MPB was required to form ICMVs (Table 1, entries 1, 7–9); the high level of reactive headgroups required for substantial ICMV yield may reflect competition between intra- (between headgroups on the same bilayer) and interbilayer crosslink formation. DTT could be replaced with DPDPB, another membrane-permeable dithiol, but not with 2 kDa PEG-dithiol (Supplementary Fig. S4 and Table 2 entries 10, 11). ICMVs could also be formed using only DOPC and MPB lipids, or using cationic 1,2-dioleoyl-3-(trimethylammonium) propane in place of DOPG (data not shown). As an alternative method to form ICMVs, maleimide-dithiol crosslinking could be replaced with bio-orthogonal click chemistry, employing alkyne-terminated lipids for vesicle formation and diazides for crosslinking[37,38] (Supplementary Fig. S5). Thus, interbilayer crosslinking for the formation of stabilized vesicles is a general strategy that can be adapted to other lipid/crosslinker chemistries. On the basis of their high synthetic yield and colloidal stability, we chose to focus on PEGylated ICMVs with a lipid composition of DOPC:DOPG:MPB in a 4:1:5 molar ratio for further testing as protein/vaccine delivery vehicles.

To test the suitability of ICMVs for protein delivery, we examined the entrapment of several globular proteins: SIV-gag, a simian analogue of human immunodeficiency virus vaccine

Table 2 | ICMV particle yield with varying synthesis conditions.

Entry	Lipid composition (molar ratio)*	Cation†	Crosslinker‡	Yield (%)§
1	DOPC/DOPG/MPB (40:10:50)	$MgCl_2$	DTT	45
2	DOPC/DOPG/MPB (40:10:50)	$CaCl_2$	DTT	50
3	DOPC/DOPG/MPB (40:10:50)	20 mM NaCl	DTT	0
4	DOPC/DOPG/MPB (40:10:50)	$MgCl_2$	-	0
5	DOPC/DOPG/MPB (40:10:50)	-	DTT	7
6	DOPC/DOPG/MPB (40:10:50)	-	15 mM DTT	4
7	DOPC/DOPG/MPB (60:15:25)	$MgCl_2$	DTT	15
8	DOPC/DOPG/MPB (72:18:10)	$MgCl_2$	DTT	0
9	DOPC/DOPG (80:20)	$MgCl_2$	DTT	0
10	DOPC/DOPG/MPB (40:10:50)	$MgCl_2$	DPDPB‖	48
11	DOPC/DOPG/MPB (40:10:50)	$MgCl_2$	HS-PEG-HS¶	3

*Hydrated with 10 mM bis-tris propane at pH 7.0. †At 10 mM unless noted otherwise. ‡At 1.5 mM unless noted otherwise. §Percentage of lipid mass recovered after synthesis and centrifugation at 14,000 *g* for 4 min. ‖1,4-Di-[3′-(2′-pyridyldithio)-propionamido]butane (molecular mass 482). ¶Molecular mass 2000.

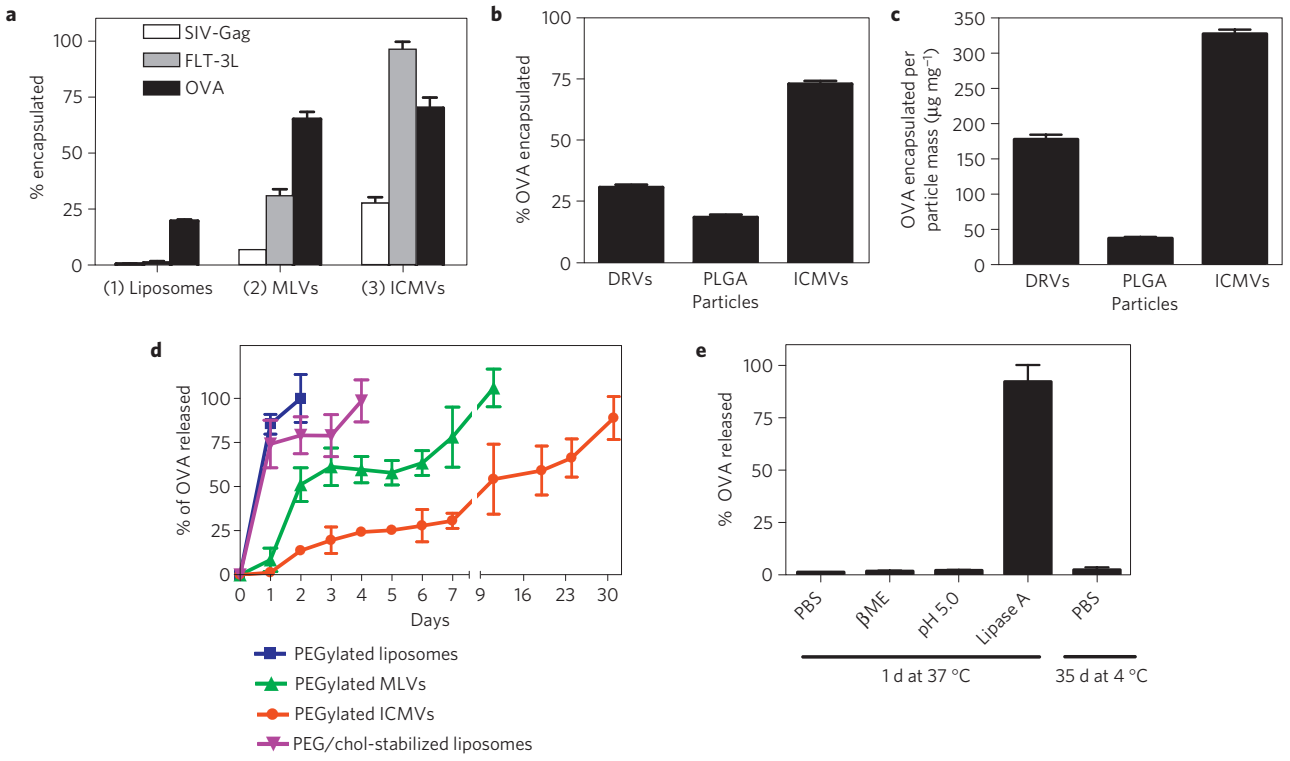

Figure 2 | Protein encapsulation and release from ICMVs. a, Encapsulation efficiency of the globular proteins SIV-gag, FLT-3L or OVA in lipid vesicles collected at each step of ICMV synthesis. **b**,**c**, Comparison of OVA encapsulation efficiency (**b**) and total protein loading per particle mass (**c**) in ICMVs versus DRVs or PLGA nanoparticles. **d**, Kinetics of OVA release from simple liposomes, MLVs or ICMVs (all with base lipid composition 4:5:1 DOPC:MPB:DOPG) incubated in RPMI medium with 10% serum at 37 °C measured over 30 d *in vitro*. Also shown for comparison are release kinetics for liposomes stabilized with cholesterol and PEG-lipid (38:57:5 DOPC:chol:PEG-DOPE). **e**, Release of OVA from ICMVs was measured in buffers simulating different aspects of the endolysomal environment: reducing buffer, 100 mM β-mercaptoethanol (β ME) in PBS; acidic buffer, 50 mM sodium citrate pH 5.0; lipase-containing buffer, 500 ng ml^{-1} lipase A in Hank's buffered saline solution. Data represent the mean ± s.e.m. of at least three experiments with $n = 3$.

antigen; FLT-3L, a therapeutic cytokine, and OVA, a model vaccine antigen. Protein encapsulation was achieved by rehydrating dried lipids with protein solutions in step (1) of the synthesis (Fig. 1a). The amount of encapsulated protein increased at each step of the ICMV preparation (Fig. 2a), which may reflect extra protein entrapment occurring as vesicle fusion occurs in both steps (2) and (3). Protein entrapment in ICMVs was not mediated by conjugation of thiols on the cargo proteins with the maleimide-functionalized lipid vesicles, as OVA prereduced with tris(2-carboxyethyl)phosphine and treated with ethyl maleimide to block all thiol groups on the protein was encapsulated in ICMVs at levels similar to those for unmodified protein (76.1 ± 6.3% versus 83.3 ± 8.4% for capped-thiol versus unmodified OVA; $p = 0.17$). We also confirmed that disulphide linkages in model protein cargos were not reduced by the DTT crosslinker during the vesicle-formation process and that ICMV encapsulation did not trigger protein aggregation (Supplementary Fig. S6). To directly compare the efficiency and quantity of protein loading achieved with ICMVs with two of the most common types of drug-delivery vehicle[39–41], we compared encapsulation of OVA in liposomes, poly(lactic-co-glycolic acid) (PLGA) nanoparticles and ICMVs: using a model stable lipid composition consisting of phosphocholine, PEG-lipid

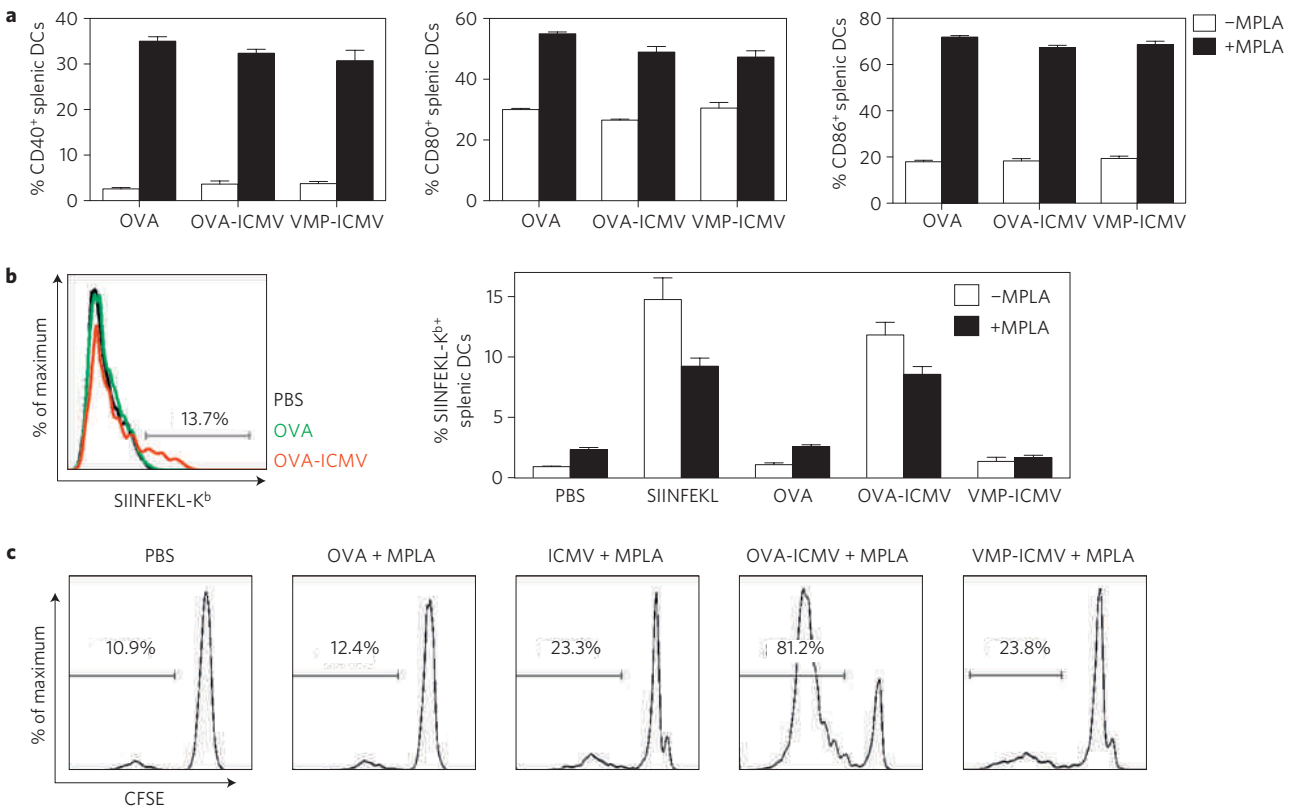

Figure 3 | *In vitro* stimulation of immune responses by ICMVs supplemented with the TLR agonist MPLA. a, Flow-cytometry analysis of expression of the cell surface costimulatory markers CD40, CD80 and CD86 on splenic DCs after 18 h incubation with 0.7 μg ml^{-1} soluble OVA, or equivalent doses of OVA loaded in ICMVs, or ICMVs loaded with an irrelevant protein (VMP), in the presence or absence of 0.1 μg ml^{-1} MPLA. **b**, Splenic DCs were incubated for 18 h with 10 μg ml^{-1} SIINFEKL peptide ($OVA_{257-264}$) and 5.0 μg ml^{-1} soluble OVA, or equivalent doses of OVA loaded in ICMVs, or VMP-loaded ICMVs in the presence or absence of 0.05 μg ml^{-1} MPLA, and the extent of cross-presentation of OVA was assessed by flow-cytometry analysis of cells stained with the 25-D1.16 mAb that recognizes SIINFEKL complexed with H-2K^b. **c**, CFSE-labelled OVA-specific naïve OT-I CD8Ts were cocultured with syngeneic splenic DCs pulsed with soluble 0.7 μg ml^{-1} OVA mixed with 0.1 μg ml^{-1} MPLA, or equivalent doses of OVA-loaded ICMVs mixed with MPLA. Empty ICMVs without antigen or ICMVs loaded with the irrelevant antigen VMP were included as negative controls. Proliferation of CD8Ts was assessed on day 3 by flow-cytometry analysis of the dilution of CFSE in the OT-I CD8Ts; shown are histograms of CFSE fluorescence. Gates on each histogram indicate the percentage of divided cells in each sample. Data represent the mean ± s.e.m. of at least three experiments with $n = 3$–4.

and cholesterol[42], we formed dehydration–rehydration vesicles (DRVs) as one of the most efficient aqueous entrapment approaches for liposomes[43], and prepared OVA-loaded PLGA particles using a double-emulsion solvent-evaporation process[44]. ICMVs exhibited superior encapsulation efficiency (~75%) compared with either DRVs or PLGA particles (two- and fourfold increases, respectively; Fig. 2b), and the amount of OVA encapsulated per total particle mass (~325 μg OVA per mg of particles) was increased in ICMVs by 1.8- and ninefold compared with DRVs or PLGA particles, respectively (Fig. 2c). Thus, ICMVs seem to be effective for encapsulating a variety of globular proteins, and, at least for the model antigen OVA, ICMVs loaded protein more efficiently than common alternative protein carriers.

We next determined whether interbilayer crosslinking enabled lipid vesicles to retain biodegradability while increasing protein retention in the presence of serum. OVA was loaded into PEGylated liposomes, Mg^{2+}-fused MLVs or ICMVs all with the same lipid composition, and the kinetics of protein release at 37 °C in media containing 10% fetal calf serum were quantified. Unilamellar liposomes quickly released their entire payload of entrapped OVA within ~2 days, whereas multilamellar Mg^{2+}-fused MLVs released ~50% of their entrapped cargo over the same time period (Fig. 2d). However, ICMVs showed a significantly enhanced retention of protein, releasing only ~25% of their cargo by one week, and ~90% after 30 days (Fig. 2d). Notably, ICMVs also released protein significantly more slowly than unilamellar liposomes stabilized by the inclusion of cholesterol[42] (Fig. 2d). The crosslinked vesicles also retained ~95% of their entrapped protein when stored in PBS at 4 °C for over 30 days (Fig. 2e). We also examined protein release from ICMVs in conditions modelling intracellular compartments: vesicles incubated in reducing or acidic conditions for 1 day at 37 °C retained >95% of entrapped OVA, whereas incubation with phospholipase A led to the release of >90% OVA and rapid vesicle degradation (Fig. 2e). Thus, ICMVs exhibit enhanced stability in the presence of serum compared with traditional liposomal formulations, but rapidly break down in the presence of enzymes that are present within intracellular endolysosomal compartments[31], providing a mechanism for triggered intracellular release of cargo following internalization by cells. Although some protein degradation within vesicles might be possible on administration *in vivo* before internalization by cells, critical uptake and processing of antigen will occur in the first few days after immunization in vaccine delivery[45], when such degradation processes should be minimal.

We hypothesized that the unique structure of ICMVs, with efficient retention of encapsulated protein antigens in the extracellular environment but rapid release in endosomes/lysosomes, would provide enhanced vaccine responses. To generate vaccine ICMVs, we prepared vesicles carrying the model antigen OVA (OVA-ICMVs) and mixed these vesicles with the molecular

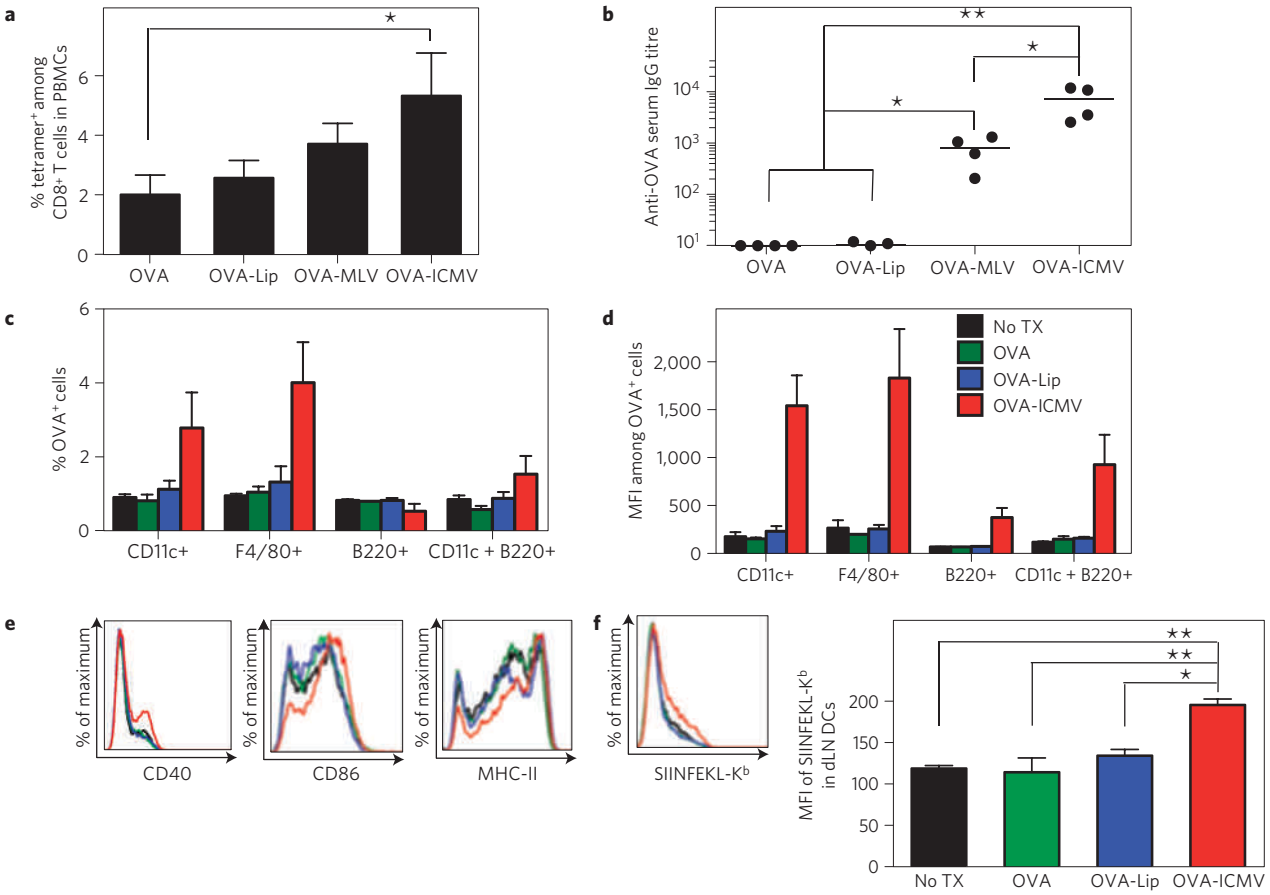

Figure 4 | *In vivo* immunization with ICMVs versus soluble antigen or antigen encapsulated in non-crosslinked vesicles. a,**b**, C57Bl/6 mice were immunized subcutaneously with a single injection of 10 μg OVA delivered in soluble, liposomal, MLV or ICMV formulations, each mixed with 0.1 μg of MPLA. **a**, The percentage of antigen-specific CD8Ts was determined by flow-cytometry analysis of PBMCs 7 days post immunization with fluorescent OVA peptide–MHC tetramers. **b**, Sera from the immunized mice were analysed by enzyme-linked immunosorbent assay 21 days post immunization for OVA-specific IgG. **c**,**d**, C57Bl/6 mice were injected with 10 μg of fluorophore-conjugated OVA mixed with 0.1 μg of MPLA as a soluble, liposomal or ICMV formulation, and the draining inguinal lymph node (dLN) cells that internalized OVA were assessed on day 2. **c**, Percentages of DCs ($CD11c^+$), macrophages ($F4/80^+$), B cells ($B220^+$) and plasmacytoid DCs ($CD11c^+B220^+$) positive for OVA uptake. **d**, The mean fluorescence intensity (MFI) of OVA^+ populations. **e**,**f**, C57Bl/6 mice were injected with 10 μg of OVA mixed with 0.1 μg of MPLA as a soluble, liposomal or ICMV formulation, and 2 d later DCs isolated from draining inguinal LNs were analysed by flow cytometry to assess DC activation and antigen cross-presentation. **e**, Overlaid histograms show costimulatory markers (CD40 and CD86) and MHC-II expression in DCs. **f**, The left panel shows overlaid histograms of inguinal LN DCs stained for SIINFEKL-K^{b+} complexes, and mean MFI levels are shown on the right panel. Data represent mean ± s.e.m. of two or three independent experiments conducted with $n = 3$–4. *, $p < 0.05$ and **, $p < 0.01$, analysed by one-way analysis of variance, followed by Tukey's HSD.

adjuvant monophosphoryl lipid A (MPLA). MPLA is a Food and Drug Administration-approved agonist for Toll-like receptor (TLR) 4 expressed by dendritic cells, B cells and innate immune cells, and potently amplifies vaccine responses[1,46]. Antigen-loaded ICMVs mixed with MPLA promoted upregulation of costimulatory molecules on splenic and bone-marrow dendritic cells (DCs) *in vitro*, compared with DCs pulsed with ICMVs without MPLA (Fig. 3a and Supplementary Fig. S7). DCs pulsed with ICMVs cross-presented peptides derived from OVA with greatly enhanced efficiency compared with those pulsed with soluble OVA (with or without added MPLA), as determined by staining DCs with the 25-D1.16 mAb that recognizes the SIINFEKL peptide ($OVA_{257–264}$) complexed with MHC class I H-$2K^b$ molecules ($p < 0.001$, compared with soluble OVA or ICMVs loaded with irrelevant antigen (vivax malaria protein, VMP), Fig. 3b). Splenic DCs incubated with OVA-ICMVs+MPLA triggered robust proliferation of OVA-specific naïve OT-1 CD8Ts *in vitro*, as assessed by a 5-(6)-carboxyfluorescein diacetate succinimidyl diester (CFSE) dilution assay. In contrast, weak T-cell responses were detected when DCs were pulsed with equivalent doses of soluble OVA and MPLA, empty ICMVs or VMP-ICMVs, indicating the specificity of the T-cell responses elicited by ICMVs (Fig. 3c). These results suggest that addition of MPLA enables equivalent DC activation by ICMVs or soluble OVA, but ICMVs trigger enhanced cross-presentation of the antigen, as expected for particulate antigen delivery.

To determine the influence of vesicle structure on the immune response *in vivo*, we vaccinated C57Bl/6 mice with equivalent doses of OVA, MPLA and lipids (10 μg, 0.1 μg and 142 μg, respectively) in the form of PEGylated unilamellar liposomes, MLVs or ICMVs. Seven days after immunization, we assessed the strength of the endogenous CD8T response by analysing the frequency of OVA peptide–MHC $tetramer^+$ (antigen-specific) CD8Ts among peripheral blood mononuclear cells (PBMCs) by flow cytometry, and found a trend toward increasing T-cell responses in the order soluble OVA < liposomes < Mg^{2+}-fused MLVs < ICMVs (Fig. 4a). At 3 weeks post-immunization, Mg^{2+}-fused MLVs elicited ~100 times greater OVA-specific IgG titres in the sera of the animals compared with soluble OVA or unilamellar liposomes. However, ICMV immunization generated a substantially stronger humoral response, ~1,000 times and ~10 times greater than the

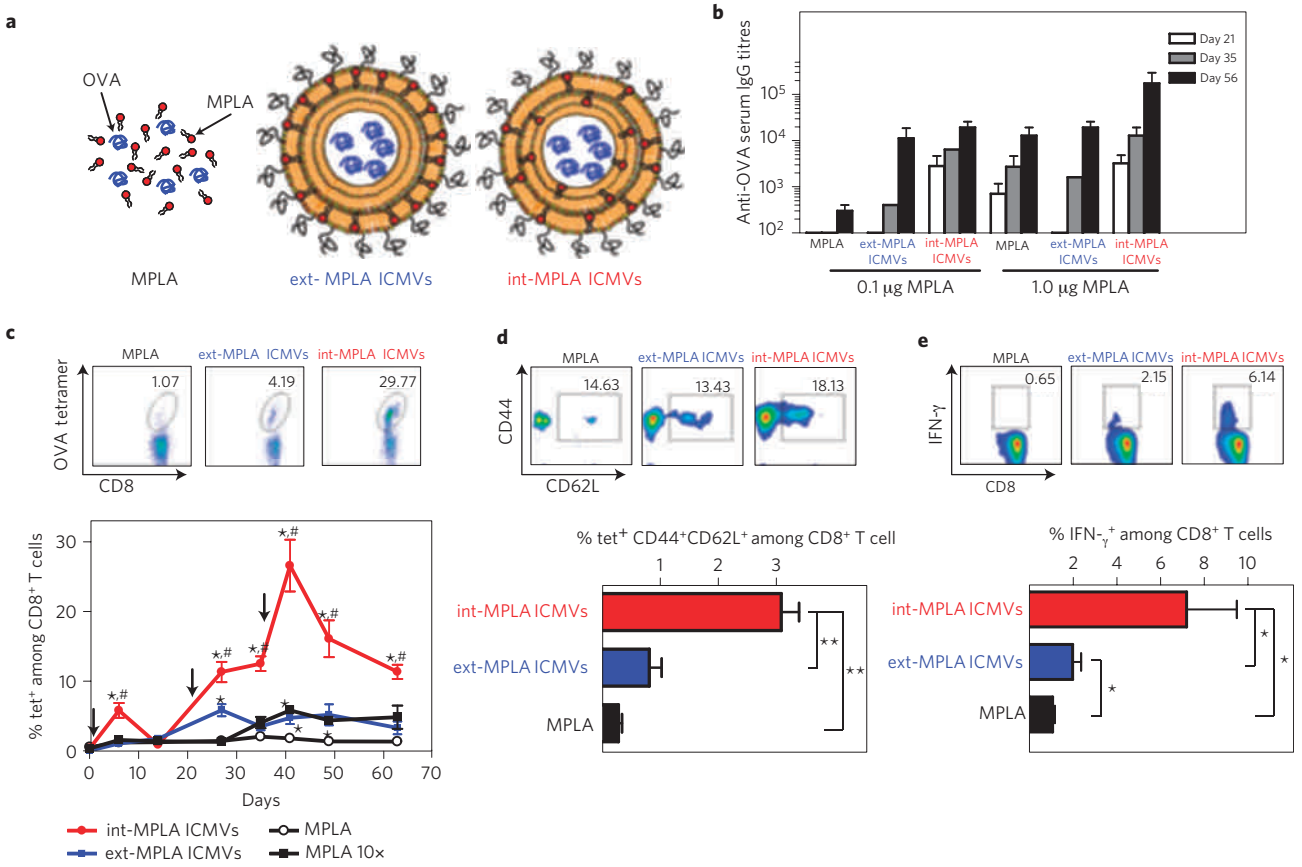

Figure 5 | ICMVs carrying antigen in the aqueous core and MPLA embedded in the vesicle walls elicit potent antibody and CD8T responses. **a**, Schematic illustration of the vaccine groups: soluble OVA mixed with MPLA (MPLA), OVA-loaded ICMVs with MPLA only on the external surface (ext-MPLA ICMVs) or OVA-loaded ICMVs with MPLA throughout the lipid multilayers (int-MPLA ICMVs). **b**–**e**, C57Bl/6 mice were immunized on days 0, 21 and 35 at the tail base subcutaneously with 10 μg OVA and either 0.1 μg or 1.0 μg of MPLA formulated as either MPLA, ext-MPLA ICMVs or int-MPLA ICMVs. **b**, Enzyme-linked immunosorbent assay analysis of total OVA-specific IgG in sera. **c**, Frequency of OVA-specific T cells in peripheral blood assessed over time through flow-cytometry analysis of tetramer$^+$CD8$^+$ T cells for vaccinations with 10 μg OVA and 0.1 μg MPLA. Response to vaccinations with soluble OVA + 1 μg MPLA (MPLA 10×) is also shown for comparison. Shown are representative flow-cytometry scatter plots from individual mice at d41 and mean tetramer$^+$ values from groups of mice versus time. **d**, Analysis of T-cell effector/effector memory/central memory phenotypes in peripheral blood by CD44/CD62L staining on tetramer$^+$ cells from peripheral blood on d41. Shown are representative cytometry plots from individual mice and mean percentages of tet$^+$CD44$^+$CD62L$^+$ cells among CD8Ts at d41. **e**, The functionality of antigen-specific CD8Ts was assayed on d49 with intracellular IFN-γ staining after *ex vivo* restimulation of PBMCs with OVA peptide *in vitro*. Representative flow-cytometry histograms of IFN-γ^+CD8$^+$ T cells from individual mice and mean results from groups are shown. Data represent the mean ± s.e.m. of two independent experiments conducted with $n = 3$. **c**, *, $p < 0.05$ compared with sol OVA + MPLA; #, $p < 0.05$ compared with ext-MPLA ICMVs. **d,e**, *, $p < 0.05$; **, $p < 0.01$, analysed by two-way analysis of variance, followed by Tukey's HSD.

soluble OVA ($p < 0.01$) and non-crosslinked MLV immunizations ($p < 0.05$), respectively (Fig. 4b). Thus, the stabilized structure of ICMVs promoted both T-cell and antibody responses. Enhanced T-cell and antibody responses to immunization with ICMVs compared with other formulations could be attributed to improved antigen delivery to antigen-presenting cells, enhanced activation of DCs, enhanced antigen cross-presentation (as seen *in vitro*) or a combination of these factors. To distinguish between these possibilities, mice were immunized with fluorophore-conjugated OVA mixed with MPLA as a soluble, liposomal or ICMV formulation, and the draining inguinal lymph node cells that internalized OVA were assessed on day 2. OVA delivered by ICMVs was readily detected in total DCs, macrophages and plasmacytoid (CD11c$^+$B220$^+$) DCs in the draining lymph nodes (dLNs), whereas soluble and liposomal formulations showed fluorescence barely above background ($p < 0.01$, Fig. 4c,d). Repeating this analysis with unlabelled OVA, we found that administration of OVA-ICMVs with MPLA triggered a minor enhancement of costimulatory marker and MHC-II expression among DCs in dLNs compared with soluble or liposomal OVA + MPLA (Fig. 4e and Supplementary Fig. S8). However, using the 25-D1.16 antibody to detect OVA peptide presentation, we readily detected OVA peptide–MHC complexes on DCs in the dLNs following ICMV immunization, whereas soluble OVA or liposomal OVA injections did not give staining above the expected background cross-reactivity of 25-D1.16 with self-peptide MHC complexes[47] (Fig. 4f). All together, these results suggest that improved retention of entrapped antigen in the crosslinked multilamellar structures of ICMVs leads to enhanced antigen delivery to antigen-presenting cells, followed by enhanced cross-presentation.

The multilamellar structure of ICMVs offers the opportunity to sequester not only protein antigen (in the aqueous core) but also lipophilic molecules (in the vesicle walls). We thus tested whether embedding MPLA throughout the walls of the ICMVs would impact the immune response *in vivo*, by enabling better retention of MPLA together with antigen in the vesicles. The TLR agonist was incorporated throughout the vesicle layers by codissolving MPLA with the other lipids in the first step of the

synthesis (int-MPLA ICMVs), and we compared these vesicles with ICMVs carrying the same amount of MPLA incorporated only on the vesicle surfaces through a post-insertion approach (ext-MPLA ICMVs, Fig. 5a, Supplementary Methods). Mice were immunized subcutaneously with OVA (10 μg) and MPLA (0.1 μg or 1.0 μg) in ICMVs or soluble form, and boosted on d21 and d35 with the same formulations. As shown in Fig. 5b, immunizations using the low dose of MPLA led to a barely detectable antibody response against soluble OVA even following two boosts, whereas both int-MPLA and ext-MPLA ICMVs elicited strong anti-OVA serum IgG titres by d56. An IgG response to soluble OVA could be obtained using ten times more MPLA, but int-MPLA ICMVs with 1.0 μg MPLA elicited higher titres than soluble protein (∼13 times greater on d56). On the other hand, we did not observe any significant level of antibodies directed against lipid components of ICMVs throughout these immunization studies (data not shown).

Embedding MPLA in the multilayers of ICMVs had a more striking effect on the CD8T response to vaccination. Soluble OVA mixed with 0.1 μg MPLA elicited barely detectable antigen-specific T-cell expansion as assessed by tetramer staining on PBMCs; ext-MPLA ICMV delivery led to a 2.5-fold increased tetramer$^+$ T-cell population by d41 (Fig. 5c, $p < 0.05$). Adding ten times more MPLA enabled soluble OVA immunizations to eventually reach T-cell responses equivalent to ext-MPLA ICMVs following boosting. By contrast, immunization with int-MPLA ICMVs elicited dramatically stronger CD8T responses that continued to expand following each boost, achieving a peak 28% tetramer$^+$ T cells in the CD8$^+$ T-cell population by d41 (five times greater than ext-MPLA ICMVs ($p < 0.05$) and 14 times greater than soluble OVA + MPLA ($p < 0.01$) Fig. 5c). Notably, int-MPLA ICMVs elicited overall a significantly higher frequency of tetramer$^+$CD44$^+$CD62L$^+$ cells ($p < 0.01$, Fig. 5d), a phenotype for central memory T cells known to confer long-lived protection against pathogens and tumours[48]. Antigen-specific T cells elicited by int-MPLA ICMVs persisted even one month after the final boosting, with ∼11% tetramer$^+$ T cells among CD8Ts (three and eight times greater than ext-MPLA ICMVs and soluble OVA + MPLA, respectively, $p < 0.05$ for both, Fig. 5c). To test the functionality of T cells expanded by these immunizations, we assessed the ability of CD8Ts from peripheral blood to produce Interferon γ (IFN-γ) on restimulation *ex vivo* on d49. Mice immunized with int-MPLA ICMVs had much higher levels of IFN-γ-competent T cells than mice receiving ext-MPLA ICMVs or soluble OVA immunizations ($p < 0.05$, Fig. 5e). To our knowledge, in terms of the degree of antigen-specific T-cell expansion, persistence of memory cells and IFN-γ functionality, this is one of the strongest endogenous T-cell responses ever reported for a protein vaccine, comparable to strong live vectors such as recombinant viruses[5,6]. Notably, this is achieved through 'homologous' boosting, repeated immunization with the same particle formulation, a strategy that cannot be used with many live vectors owing to immune responses raised against the pathogen-based delivery vector itself[7].

These studies demonstrate the synthesis of a new class of submicrometre-particle reagents based on crosslinked multilamellar lipid vesicles, which combine a number of attractive features for biomedical applications: the particle synthesis does not require exposure of protein cargos to organic solvents, the lipid basis of the particles makes them inherently biodegradable to metabolizable by-products, the phospholipid shell enables modular entrapment of both lipophilic and hydrophilic cargos, proteins are encapsulated at very high levels per mass of particles and protein release from the particles can be sustained over very long durations. These results suggest that ICMVs may be a very effective vehicle for delivering biomacromolecules, and in particular for vaccine applications. The ability to achieve such strong combined T-cell and antibody responses using a synthetic-particle vaccine could open up new possibilities for vaccination in the setting of infectious disease and cancer.

Materials and methods

Synthesis of ICMVs. 1.26 μmol of lipids in chloroform (typical lipid composition DOPC:DOPG:MPB = 4:1:5 molar ratio, all lipids from Avanti Polar Lipids, Alabaster, AL) were dispensed to glass vials, and the organic solvents were evaporated under vacuum overnight to prepare dried thin lipid films. The lipid films were rehydrated in 10 mM bis–tris propane at pH 7.0 with cargo proteins for 1 h with rigorous vortexing every 10 min, and then sonicated in alternating power cycles of 6 W and 3 W in 30 s intervals for 5 min on ice (Misonix Microson XL probe tip sonicator, Farmingdale, NY). The liposomes formed in this first step were induced to undergo fusion by addition of divalent cations such as Mg^{2+} and Ca^{2+} at a final concentration of 10 mM. The resulting MLVs were incubated with 1.5 mM DTT (maleimide:DTT molar ratio of 2:1) for 1 h at 37 °C to conjugate opposing bilayers of maleimide-functionalized lipids and form crosslinked ICMVs; the resulting vesicles were recovered by centrifugation at 14,000 × g for 4 min, and washed twice with deionized water. For PEGylation, the particles were incubated with 2 kDa PEG-SH (Laysan Bio, Arab, AL) in a 1.5-fold molar excess of PEG-SH to maleimide groups for 1 h at 37 °C. The resulting particles were centrifuged and washed 3× with deionized water. The final products were either stored in PBS at 4 °C or lyophilized in the presence of 3% sucrose as a cryoprotectant and stored at −20 °C. For some assays, simple liposomes or Mg-fused MLVs were harvested before crosslinking with ultracentrifugation at 115,000 *g* using an Optima ultracentrifuge for 6 h (Beckman Coulter).

***In vitro* protein loading and drug release.** For encapsulation studies, ovalbumin (OVA, Worthington, Lakewood, NJ), SIV-gag (Advanced Bioscience Laboratories, Kensington, MD) and FLT-3L (Peprotech, Rocky Hill, NJ) were labelled with Alexa-Fluor 555 (Invitrogen, Carlsbad, CA) for direct fluorometric quantification of the amount of protein entrapped. OVA was also encapsulated in DRVs and PLGA nanoparticles as described previously[43,44]. In some experiments, ICMVs were loaded with a recombinant VMP as an irrelevant antigen control[49] (provided by A. Yadava, Walter Reed Army Institute of Research). Capped-thiol OVA was prepared by incubating 1 mg of OVA with 1.5 mM tris(2-carboxyethyl)phosphine for 1 h at RT, followed by incubation with 1.5 mM ethyl maleimide (Pierce, Rockford, IL) at 37 °C for 1 h. The extent of thiol protection was >95% as assessed with Ellman's assay[50]. Release of OVA labelled with Alexa-Fluor 555 from lipid vesicles was quantified in RPMI (Roswell Park Memorial Institute) medium supplemented with 10% fetal calf serum at 37 °C using dialysis membranes with a molecular mass cutoff of 100 kDa. At regular intervals, the releasing media were removed for quantification of fluorescence, and an equal volume of fresh medium was replaced for continued monitoring of drug release. Residual OVA remaining at the end of the time-course was determined by lipid extraction of vesicles with 1% Triton X-100 treatment and measuring released protein by fluorescence spectrophotometry. OVA release assays were also carried out in Hank's buffered saline solution supplemented with 500 ng ml^{-1} of phospholipase A (Sigma, St Louis, MO). To examine the stability of encapsulated cargo molecules, monoclonal rat IgG encapsulated in ICMVs was retrieved with 1% Triton X-100 treatment and analysed with SDS-PAGE under non-reducing conditions with silver staining (Pierce).

Vaccination study with ICMVs. Groups of C57Bl/6 mice (Jackson Laboratories) were immunized subcutaneously in the tail base with indicated doses of OVA (with or without TLR agonists, MPLA). Frequencies of OVA-specific CD8Ts and their phenotypes elicited by immunization were determined by flow-cytometry analysis of PBMCs at selected time points following staining with 4,6-diamidino-2-phenylindole (to discriminate live/dead cells), anti-CD8 α, anti-CD44, anti-CD62L and SIINFEKL/H-2K^b peptide–MHC tetramers (Becton Dickinson). To assess the functionality of primed CD8Ts, PBMCs were stimulated *ex vivo* with 1 μM OVA-peptide SIINFEKL for 6 h with GolgiPlug (Becton Dickinson), fixed, permeabilized, stained with anti- IFN-γ and CD8 α, and analysed by flow cytometry. Anti-OVA IgG titres, defined as the dilution of sera at which the 450 nm OD reading is 0.5, were determined by enzyme-linked immunosorbent assay analysis of sera from immunized mice. Animals were cared for following National Institutes of Health, state and local guidelines.

Statistical analysis. Statistical analysis was carried out with Jmp 5.1 (SAS Institute, Cary, NC). Data sets were analysed using one- or two-way analysis of variance, followed by Tukey's HSD test for multiple comparisons. *p*-values less than 0.05 were considered statistically significant. All values are reported as mean ± s.e.m.

Received 23 August 2010; accepted 11 January 2011; published online 20 February 2011

References

1. Guy, B. The perfect mix: Recent progress in adjuvant research. *Nature Rev. Microbiol.* **5,** 505–517 (2007).
2. Perrie, Y., Mohammed, A. R., Kirby, D. J., McNeil, S. E. & Bramwell, V. W. Vaccine adjuvant systems: Enhancing the efficacy of sub-unit protein antigens. *Int. J. Pharm.* **364,** 272–280 (2008).

3. Reed, S. G., Bertholet, S., Coler, R. N. & Friede, M. New horizons in adjuvants for vaccine development. *Trends Immunol.* **30,** 23–32 (2009).
4. Walker, B. D. & Burton, D. R. Toward an AIDS vaccine. *Science* **320,** 760–764 (2008).
5. Haglund, K. *et al.* Robust recall and long-term memory T-cell responses induced by prime-boost regimens with heterologous live viral vectors expressing human immunodeficiency virus type 1 Gag and Env proteins. *J. Virol.* **76,** 7506–7517 (2002).
6. Flatz, L. *et al.* Development of replication-defective lymphocytic choriomeningitis virus vectors for the induction of potent $CD8^+$ T cell immunity. *Nature Med.* **16,** 339–345 (2010).
7. Brave, A., Ljungberg, K., Wahren, B. & Liu, M. A. Vaccine delivery methods using viral vectors. *Mol. Pharm.* **4,** 18–32 (2007).
8. Priddy, F. H. *et al.* Safety and immunogenicity of a replication-incompetent adenovirus type 5 HIV-1 clade B gag/pol/nef vaccine in healthy adults. *Clin. Infect. Dis.* **46,** 1769–1781 (2008).
9. Hubbell, J. A., Thomas, S. N. & Swartz, M. A. Materials engineering for immunomodulation. *Nature* **462,** 449–460 (2009).
10. Heath, W. R. & Carbone, F. R. Cross-presentation in viral immunity and self-tolerance. *Nature Rev. Immunol.* **1,** 126–134 (2001).
11. Kwon, Y. J., James, E., Shastri, N. & Frechet, J. M. *In vivo* targeting of dendritic cells for activation of cellular immunity using vaccine carriers based on pH-responsive microparticles. *Proc. Natl Acad. Sci. USA* **102,** 18264–18268 (2005).
12. Hamdy, S. *et al.* Enhanced antigen-specific primary $CD4^+$ and $CD8^+$ responses by codelivery of ovalbumin and toll-like receptor ligand monophosphoryl lipid A in poly(D,L-lactic-co-glycolic acid) nanoparticles. *J. Biomed. Mater. Res. A* **81,** 652–662 (2007).
13. Heit, A., Schmitz, F., Haas, T., Busch, D. H. & Wagner, H. Antigen co-encapsulated with adjuvants efficiently drive protective T cell immunity. *Eur. J. Immunol.* **37,** 2063–2074 (2007).
14. Schlosser, E. *et al.* TLR ligands and antigen need to be coencapsulated into the same biodegradable microsphere for the generation of potent cytotoxic T lymphocyte responses. *Vaccine* **26,** 1626–1637 (2008).
15. Heffernan, M. J., Kasturi, S. P., Yang, S. C., Pulendran, B. & Murthy, N. The stimulation of $CD8^+$ T cells by dendritic cells pulsed with polyketal microparticles containing ion-paired protein antigen and poly(inosinic acid)-poly(cytidylic acid). *Biomaterials* **30,** 910–918 (2009).
16. Demento, S. L. *et al.* Inflammasome-activating nanoparticles as modular systems for optimizing vaccine efficacy. *Vaccine* **27,** 3013–3021 (2009).
17. Reddy, S. T. *et al.* Exploiting lymphatic transport and complement activation in nanoparticle vaccines. *Nature Biotechnol.* **25,** 1159–1164 (2007).
18. Torchilin, V. P. Recent advances with liposomes as pharmaceutical carriers. *Nature Rev. Drug Discov.* **4,** 145–160 (2005).
19. Gregoriadis, G., Gursel, I., Gursel, M. & McCormack, B. Liposomes as immunological adjuvants and vaccine carriers. *J. Control. Release* **41,** 49–56 (1996).
20. Jeong, J. M., Chung, Y. C. & Hwang, J. H. Enhanced adjuvantic property of polymerized liposome as compared to a phospholipid liposome. *J. Biotechnol.* **94,** 255–263 (2002).
21. Vangala, A. *et al.* Comparison of vesicle based antigen delivery systems for delivery of hepatitis B surface antigen. *J. Control. Release* **119,** 102–110 (2007).
22. Steers, N. J., Peachman, K. K., McClain, S., Alving, C. R. & Rao, M. Liposome-encapsulated HIV-1 Gag p24 containing lipid A induces effector $CD4^+$ T-cells, memory $CD8^+$ T-cells, and pro-inflammatory cytokines. *Vaccine* **27,** 6939–6949 (2009).
23. Bhowmick, S., Mazumdar, T., Sinha, R. & Ali, N. Comparison of liposome based antigen delivery systems for protection against *Leishmania donovani*. *J. Control. Release* **141,** 199–207 (2010).
24. Reddy, R., Zhou, F., Nair, S., Huang, L. & Rouse, B. T. *In vivo* cytotoxic T lymphocyte induction with soluble proteins administered in liposomes. *J. Immunol.* **148,** 1585–1589 (1992).
25. Collins, D. S., Findlay, K. & Harding, C. V. Processing of exogenous liposome-encapsulated antigens *in vivo* generates class I MHC-restricted T cell responses. *J. Immunol.* **148,** 3336–3341 (1992).
26. Wakita, D. *et al.* An indispensable role of type-1 IFNs for inducing CTL-mediated complete eradication of established tumor tissue by CpG-liposome co-encapsulated with model tumor antigen. *Int. Immunol.* **18,** 425–434 (2006).
27. Popescu, M. C. *et al.* A novel proteoliposomal vaccine elicits potent antitumor immunity in mice. *Blood* **109,** 5407–5410 (2007).
28. Allen, T. M., Mumbengegwi, D. R. & Charrois, G. J. Anti-CD19-targeted liposomal doxorubicin improves the therapeutic efficacy in murine B-cell lymphoma and ameliorates the toxicity of liposomes with varying drug release rates. *Clin. Cancer. Res.* **11,** 3567–3573 (2005).
29. Cashion, M. P. & Long, T. E. Biomimetic design and performance of polymerizable lipids. *Acc. Chem. Res.* **42,** 1016–1025 (2009).
30. Hotz, J. & Meier, W. Vesicle-templated polymer hollow spheres. *Langmuir* **14,** 1031–1036 (1998).
31. Mahadevan, S. & Tappel, A. L. Lysosomal lipases of rat liver and kidney. *J. Biol. Chem.* **243,** 2849–2854 (1968).
32. Papahadjopoulos, D., Nir, S. & Duzgunes, N. Molecular mechanisms of calcium-induced membrane fusion. *J. Bioenerg. Biomembr.* **22,** 157–179 (1990).
33. Zauner, W., Farrow, N. A. & Haines, A. M. *In vitro* uptake of polystyrene microspheres: Effect of particle size, cell line and cell density. *J. Control. Release* **71,** 39–51 (2001).
34. Mohammed, A. R., Bramwell, V. W., Coombes, A. G. & Perrie, Y. Lyophilisation and sterilisation of liposomal vaccines to produce stable and sterile products. *Methods* **40,** 30–38 (2006).
35. Girard, P. *et al.* A new method for the reconstitution of membrane proteins into giant unilamellar vesicles. *Biophys. J.* **87,** 419–429 (2004).
36. Lutsiak, M. E., Robinson, D. R., Coester, C., Kwon, G. S. & Samuel, J. Analysis of poly(D,L-lactic-co-glycolic acid) nanosphere uptake by human dendritic cells and macrophages *in vitro*. *Pharm. Res.* **19,** 1480–1487 (2002).
37. Huisgen, R. Cycloadditions—definition classification and characterization. *Angew. Chem. Int. Ed.* **7,** 321 (1968).
38. Wang, Q. *et al.* Bioconjugation by copper(I)-catalyzed azide-alkyne [3 + 2] cycloaddition. *J. Am. Chem. Soc.* **125,** 3192–3193 (2003).
39. Allen, T. M. & Cullis, P. R. Drug delivery systems: Entering the mainstream. *Science* **303,** 1818–1822 (2004).
40. Mundargi, R. C., Babu, V. R., Rangaswamy, V., Patel, P. & Aminabhavi, T. M. Nano/micro technologies for delivering macromolecular therapeutics using poly(D,L-lactide-co-glycolide) and its derivatives. *J. Control. Release* **125,** 193–209 (2008).
41. Vasir, J. K. & Labhasetwar, V. Biodegradable nanoparticles for cytosolic delivery of therapeutics. *Adv. Drug Deliv. Rev.* **59,** 718–728 (2007).
42. Gabizon, A. *et al.* Prolonged circulation time and enhanced accumulation in malignant exudates of doxorubicin encapsulated in polyethylene-glycol coated liposomes. *Cancer Res.* **54,** 987–992 (1994).
43. Kirby, C. & Gregoriadis, G. Dehydration–rehydration vesicles—a simple method for high-yield drug entrapment in liposomes. *Bio/Technology* **2,** 979–984 (1984).
44. Bershteyn, A. *et al.* Polymer-supported lipid shells, onions, and flowers. *Soft Matter* **4,** 1787–1791 (2008).
45. McKee, A. S., Munks, M. W. & Marrack, P. How do adjuvants work? Important considerations for new generation adjuvants. *Immunity* **27,** 687–690 (2007).
46. Mata-Haro, V. *et al.* The vaccine adjuvant monophosphoryl lipid A as a TRIF-biased agonist of TLR4. *Science* **316,** 1628–1632 (2007).
47. Porgador, A., Yewdell, J. W., Deng, Y., Bennink, J. R. & Germain, R. N. Localization, quantitation, and *in situ* detection of specific peptide–MHC class I complexes using a monoclonal antibody. *Immunity* **6,** 715–726 (1997).
48. Sallusto, F., Geginat, J. & Lanzavecchia, A. Central memory and effector memory T cell subsets: Function, generation, and maintenance. *Annu. Rev. Immunol.* **22,** 745–763 (2004).
49. Yadava, A. *et al.* A novel chimeric *Plasmodium vivax* circumsporozoite protein induces biologically functional antibodies that recognize both VK210 and VK247 sporozoites. *Infect. Immun.* **75,** 1177–1185 (2007).
50. Ellman, G. L. Tissue sulfhydryl groups. *Arch. Biochem. Biophys.* **82,** 70–77 (1959).

Acknowledgements

This work was supported in part by the Ragon Institute of MGH, MIT and Harvard, the Gates Foundation, the Department. of Defense (contract W911NF-07-D-0004) and the National Institutes of Health (P41RR002250 and RC2GM092599). The authors would like to thank A. Yadava for providing the VMP antigen. D.J.I. is an investigator of the Howard Hughes Medical Institute.

Author contributions

J.J.M. and D.J.I. designed the experiments. J.J.M. carried out the experiments; H.S. assisted in the *in vivo* characterization and immunization studies. A.B., H.K., J.T.G., J.R. and W.C. contributed cryoelectron microscope imaging. M.T.S. and S.H.U. contributed experimental suggestions. H.L., B.H., M.S. and S.L. provided technical support. J.J.M. and D.J.I. analysed the data and wrote the paper.

Additional information

The authors declare no competing financial interests. Supplementary information accompanies this paper on www.nature.com/naturematerials. Reprints and permissions information is available online at http://npg.nature.com/reprintsandpermissions. Correspondence and requests for materials should be addressed to D.J.I.

nature materials

SUPPLEMENTARY INFORMATION

DOI: 10.1038/NMAT2960

Interbilayer-Crosslinked Multilamellar Vesicles as Synthetic Vaccines for Potent Humoral and Cellular Immune Responses

James J. Moon, Heikyung Suh, Anna Bershteyn, Matthias T. Stephan, Haipeng Liu, Bonnie Huang, Mashaal Sohail, Samantha Luo, Soong Ho Um, Htet Khant, Jessica T. Goodwin, Jenelyn Ramon, Wah Chiu, and Darrell J. Irvine

Correspondence should be addressed to D.J.I. (djirvine@mit.edu)

DOI: 10.1038/NMAT2960

SUPPLEMENTARY METHODS

Characterization of ICMVs. Particle size and surface charge were determined by dynamic light scattering (DLS) using a 90Plus/ZetaPals particle size and ξ-potential analyzer (Brookhaven Instruments). To quantify the fraction of lipids exposed on the external surfaces of particles, a lamellarity assay was performed as described previously[1]. Maleimide and thiol content on the external surface of particles were quantified using fluorimetric quantification kits (ATT Bioquest, Sunnyvale, CA).

Cryoelectron Microscopy. The particles were analyzed using cryoelectron microscopy[2]. A holey carbon-film grid (Quantifoil Micro Tools GmbH, Jena, Germany) was pretreated with Gatan Solarus 950 plasma cleaner. Three μl of the specimen was applied to the grid, and plunge frozen in liquid ethane using Gatan Cryoplunge 3 (Gatan Inc, Pleasanton, CA, USA). Low dose imaging of the frozen, hydrated specimen kept at liquid nitrogen temperature with a Gatan 626 single tilt cryoholder was performed on a JEM2100 electron microscope (JEOL Ltd, Tokyo, Japan) operating at 200kV. All images were recorded at ~40,000x magnification using a Gatan UltraScan 4000 CCD camera.

Thin layer chromatography. To examine crosslinking of maleimide-functionalized lipids, individual lipid components and lipid vesicles before and after interbilayer-crosslinking were dissolved in chloroform, and 5 μL of the lipids solution was spotted on TLC plate and developed with $CHCl_3$/MeOH/H_2O/NH_4OH (40:15:2:1). The TLC plate was then dried and visualized with anisaldehyde staining solution.

Synthesis of alkyne-modified lipids and ICMV formation with alkyne-azide chemistry. 744 mg 1,2-dioleoyl-*sn*-glycero-3-phosphoethanolamine (DOPE, 1 mmol) was mixed with

N-hydroxysuccinimide ester of propiolic acid (167 mg, 1 mmol) and Et_3N (202 mg, 2 mmol) in 5 mL $CDCl_3$, and the reaction was monitored by NMR. After 3 hours at room temperature, the reaction was completed. After the organic solution was washed with 5 mL 5% Na_2CO_3, 1% HCl and brine, dried under Na_2SO_4 and evaporated, alkyne-modified DOPE was weighed. 1.26 μmol of lipid film with DOPC and alkyne-DOPE in 1:1 molar ratio was prepared, hydrated, sonicated, and induced to fuse with 10 mM Mg^{2+} as described previously. MLVs with alkyne-functionalized lipids were incubated with 2.5 mM $CuSO_4$, copper wire, and 1.5 mM 1, 14-diazido-3,6,9,12-tetraoxatetradecane for 24 hrs at RT. Particle yield was measured after 3X washes with centrifugation.

Incorporation of MPLA in ICMVs. MPLA was incorporated throughout multilayers in ICMVs (int-MPLA ICMVs) by pre-mixing MPLA in lipid film and following the normal synthesis protocol for ICMV and PEGylation. To load MPLA externally on ICMVs (ext-MPLA ICMVs), MPLA was incubated with PEGylated, plain ICMVs for 30 min at 37˚C and then washed twice in diH_2O with centrifugation. The incorporation efficiencies of MPLA were 56 ± 2.2% and 14.5 ± 2.3% in int-MPLA and ext-MPLA ICMVs, respectively, as measured with dansyl-modified MPLA. (MPLA was modified with dansylhydrazine as described previously[3]. Briefly, MPLA was dissolved in 1 mL $CHCl_3$/MeOH (3:1) with 10 μL TFA, and added with 5 mg of danzylhydrazine (Sigma-aldrich) dissolved in 200 μL EtOH. The reaction mixture was sealed and heated at 70°C for 6 hours. After cooling down to room temperature, the solvent was evaporated under a stream of N_2 and dried under vacuum. The product was washed with cold acetone (3x0.5mL) and purified by silica gel chromatography.) The amount of MPLA added for each method was adjusted to normalize the final amount of MPLA incorporated in ICMVs.

DOI: 10.1038/NMAT2960

***In vitro* activation study with dendritic cells and CD8$^+$ T-cells.**

To examine activation of DCs by ICMVs *in vitro*, we used DCs freshly isolated from spleens of 6-10 wk old C57Bl/6 mice and enriched with an anti-CD11c MACS isolation kit (Stem Cell Technologies, Vancouver, BC, Canada). 4x10^5 splenic DCs were incubated with 0.7 μg/ml of soluble OVA, equivalent doses of OVA loaded in ICMVs, or ICMVs loaded with VMP in the presence or absence of 0.1 μg/ml MPLA. After 18 hrs, cells were analyzed by flow cytometry to examine the extent of DC maturation following staining with anti-CD11c, CD40, CD80, and CD86. To assess the extent of antigen cross-presentation, splenic DCs incubated for 18 hr with 10 μg/mL SIINFEKL peptide ($OVA_{257-264}$), 5.0 μg/mL soluble OVA, equivalent doses of OVA loaded in ICMVs, or VMP-loaded ICMVs in the presence or absence of 0.05 μg/mL MPLA were stained with 25-D1.16 mAb (Ebioscience, San Diego, CA) and analyzed with flow cytometry. Cross-priming of CD8$^+$ T-cells by syngeneic splenic DCs was examined *in vitro*. 2x10^4 splenic DCs were pulsed for 4 hrs with 0.7 μg/ml of OVA formulated either in ICMVs or solution with or without 0.1 μg/ml of MPLA, and then co-cultured with 5x10^4 5-(6)-carboxyfluorescein diacetate succinimidyl diester (CFSE)-labeled OVA-specific naïve OT-I CD8$^+$ T-cells. After 3 d, proliferation of CD8$^+$ T-cells was assessed by flow cytometry analysis of the dilution of CFSE in the OT-I CD8$^+$ T-cells.

In some experiments, bone marrow-derived DCs (BMDCs) isolated and cultured as reported previously[4] were also used to assess activation of DCs. Briefly, bone marrow was isolated from 6-10 wk old C57Bl/6 mice, and the cells were passed through a 70 μm cell strainer, washed, and plated on non-TC Petri dish with 20 ng/ml granulocyte monocyte-colony stimulating factor (GM-CSF) (Peprotech). The culture media was changed on days 3, 6, and 8 with media supplemented with 20 ng/ml GM-CSF. On d10, 4x10^5 BMDCs were incubated with 3.3 μg/ml of OVA loaded in ICMVs with or without addition of 0.36 μg/ml MPLA. After 18 hrs, cells were analyzed by flow cytometry to examine the extent of DC

maturation following staining with anti-CD11c, CD40, CD86, and MHC-II.

Draining of OVA-loaded particles and activation of DCs *in vivo.* Fluorophore-tagged OVA was synthesized by reacting OVA with Alexa Fluor 647-succinimidyl ester (Invitrogen, Carlbad, CA). C57Bl/6 mice were immunized at tail base s.c. with a single injection of 10 μg fluorophore-tagged OVA and 0.1 μg of MPLA as a soluble, liposomal, or ICMV formulation. After 2 d, draining inguinal lymph nodes were isolated and digested with 100 Mandl U/ml collagenase D for 60 min at RT (Roche, Mannheim, Germany). After passing the lymph node cells through 70 μm cell strainer and washing, the cells were stained with DAPI, anti-CD11c, anti-F4/80, and anti-B220 (Ebioscience) and analyzed with flow cytometry. To examine activation of DCs by ICMV *in vivo,* C57Bl/6 mice were injected at tail base s.c. with 10 μg of OVA mixed with 0.1 μg of MPLA as a soluble, liposomal, or ICMV formulation, and 2 d later, DCs were isolated from draining inguinal lymph nodes and processed to individual cells as mentioned above. After staining the cells with 25-D1.16 mAb, anti-CD11c, anti-CD40, anti-CD86, and anti-MHC-II, they were analyzed with flow cytometry.

DOI: 10.1038/NMAT2960

SUPPLEMENTARY FIGURE LEGENDS

Supplementary Figure 1. Quenching of available maleimide and thiol groups on the surfaces of ICMVs following DTT treatment and PEG-thiol capping. Percentage of external lipids with **a,** reactive maleimide or **b,** free thiol groups were measured using fluorimetric assays following exposure of MLVs to DTT and PEG-thiol (see Methods). **a,** After interbilayer-crosslinking of Mg^{2+}-fused MLVs with 1.5 mM DTT, the resulting ICMVs had less than 3% of lipids with reactive maleimide groups, which decreased further with subsequent PEG-thiol treatment. **b,** Percentage of external lipids with thiol groups remained minimal (< 0.05 %) during ICMV synthesis, indicating absence of DTT-lipid conjugates with unreacted thiol groups on the external surfaces of ICMVs.

Supplementary Figure 2. CryoEM images of ICMVs. a-d, Additional representative cryo-EM images show examples of the thick, multilayered lipid walls formed in ICMVs. Arrow in **d** highlights an example of incomplete external lipid layers seen infrequently in ICMV vesicles. Scale bars = 100 nm.

Supplementary Figure 3. Thin layer chromatography analysis of the crosslinked lipids in ICMVs. Migration patterns of lipids from interbilayer-crosslinked ICMVs were compared to those of non-crosslinked Mg^{2+}-fused liposomes (MLVs) and the individual lipid components (see Supplementary Methods). Arrow at right highlights the position of a unique band seen in lane 4 shifted from the position of monomeric MPB lipids, suggesting successful conjugation of maleimide-functionalized lipids with the dithiol crosslinker.

Supplementary Figure 4. Structures of alternative dithiol crosslinkers tested for ICMV synthesis (cited in Table 2).

Supplementary Figure 5. Alternative interbilayer-crosslinked reaction using "click" chemistry. **a**, An alkyne-headgroup lipid was synthesized from DOPE and an alkyne precursor (see Supplementary Methods). **b**, Liposomes were formed with alkyne-terminated lipids and induced to form MLVs by Mg^{2+}. Subsequent incubation of the alkyne-bearing MLVs with diazide and catalyst as indicated led to successful formation of ICMVs with 83% particle yield, as measured after particle retrieval with low-speed centrifugation conditions.

Supplementary Figure 6. Proteins encapsulated in ICMVs do not undergo chemical modification. To assess the stability of the disulfide linkages in encapsulated proteins, ICMVs loaded with a monoclonal rat IgG antibody were lysed with Triton X-100, and the recovered protein was analyzed by SDS-PAGE under non-reducing conditions. The untreated stock antibody (mAb) showed a major band near 150 kDa, while antibody treated with 10 mM DTT for 30 min (mAb + DTT) showed nearly complete reduction into heavy (50 kDa) and light chain (25 kDa) components. In contrast, IgG recovered from ICMVs was indistinguishable from the unmodified starting material, suggesting that proteins do not undergo significant chemical modification or aggregation during encapsulation in ICMVs.

Supplementary Figure 7. Stimulation of bone marrow-derived DCs by ICMVs supplemented with the TLR agonist MPLA. Bone marrow-derived DCs (BMDCs) were incubated for 18 hr with 3.3 μg/ml of OVA in ICMVs in the presence or absence of 0.36 μg/mL MPLA, and the expression levels of the cell surface costimulatory markers (CD40 and CD86) and MHC-II were analyzed with flow cytometry.

DOI: 10.1038/NMAT2960

Supplementary Figure 8. *In vivo* stimulation of DCs by ICMVs mixed with MPLA. C57Bl/6 mice were injected with 10 μg of OVA mixed with 0.1 μg of MPLA as a soluble, liposomal, or ICMV formulation, and 2 d later, DCs isolated from draining inguinal LNs were analyzed with flow cytometry for costimulation markers (CD40 and CD86) and MHC-II.

SUPPLEMENTARY REFERENCES

1. Girard, P. et al. A new method for the reconstitution of membrane proteins into giant unilamellar vesicles. *Biophys. J.* **87**, 419-429 (2004).
2. Baker, M. L., Marsh, M. P. & Chiu, W. *Nanotechnology: Cryo-EM of molecular nanomachines and cells*. (Wiley VCH, Weinheim, 2009).
3. Shilova, N. V. & Bovin, N. V. Fluorescent labels for the analysis of mono- and oligosaccharides. *Russian Journal of Bioorganic Chemistry* **29**, 309-324 (2003).
4. Lutz, M. B. et al. An advanced culture method for generating large quantities of highly pure dendritic cells from mouse bone marrow. *J. Immunol. Methods* **223**, 77-92 (1999).

Sup. Fig. 1

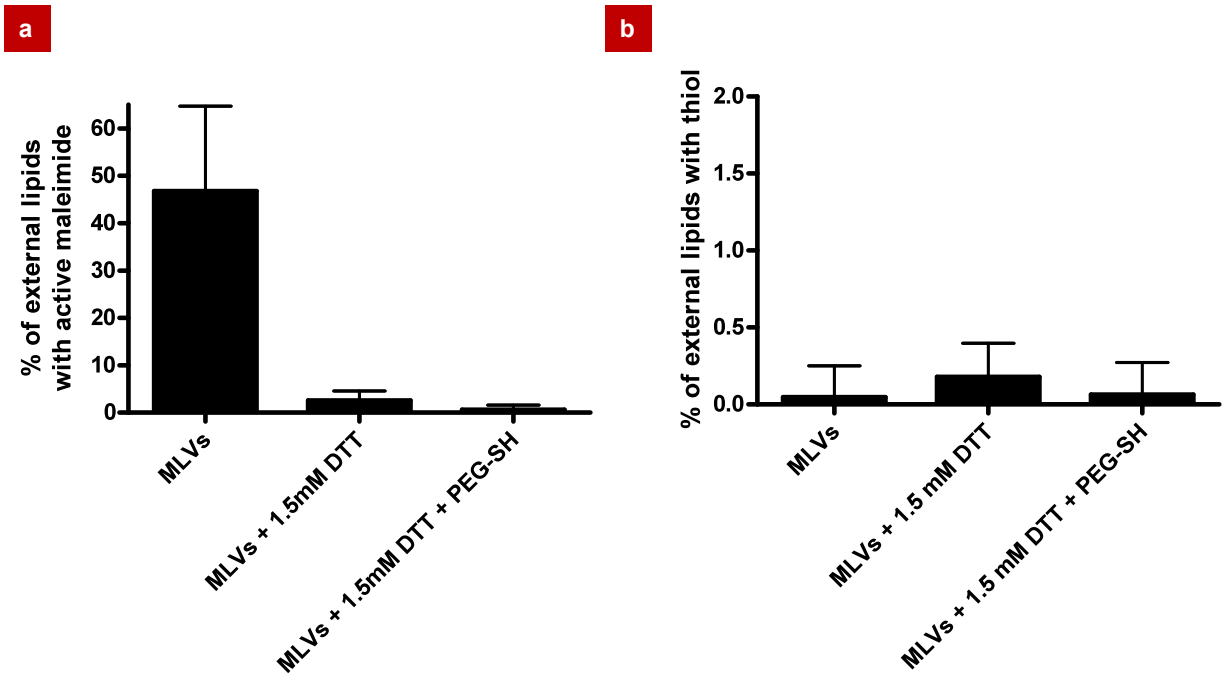

DOI: 10.1038/NMAT2960

Sup. Fig. 2

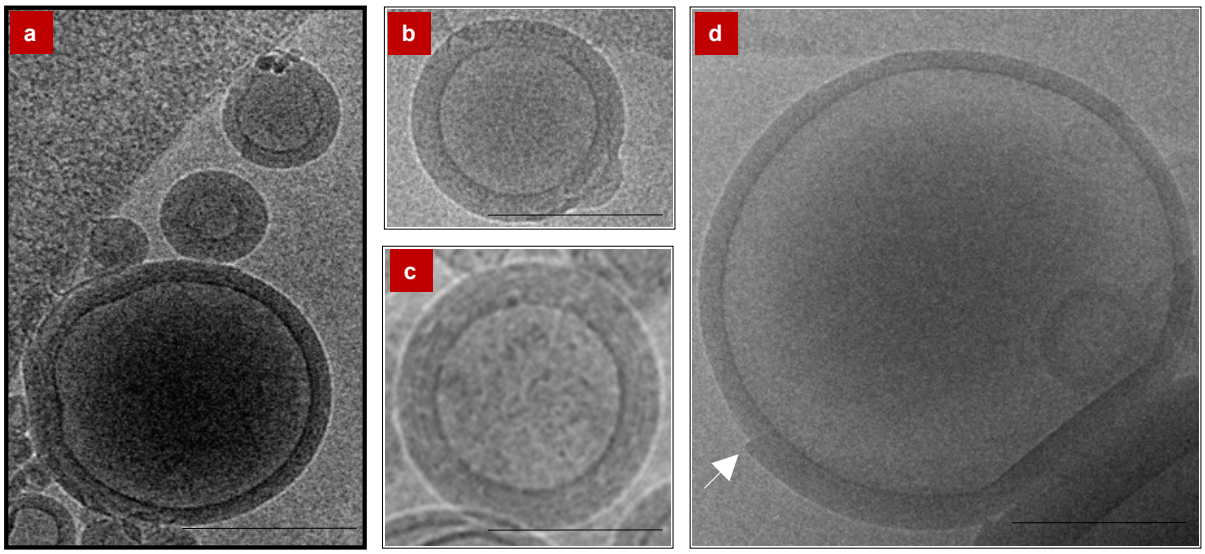

Sup. Fig. 3

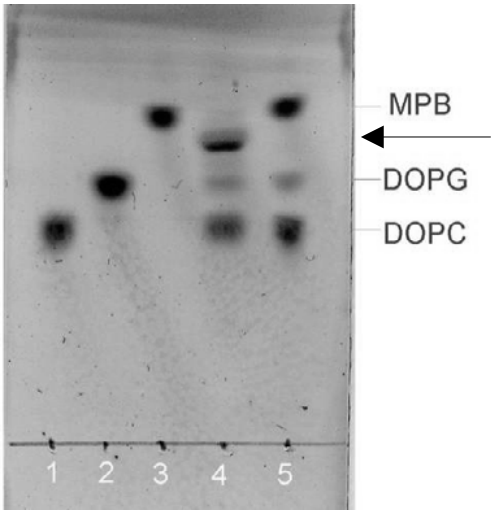

1. DOPC lipid alone
2. DOPG lipid alone
3. MPB lipid alone
4. MLVs following DTT crosslinking (ICMVs)
5. MLVs

DOI: 10.1038/NMAT2960

Sup. Fig. 4

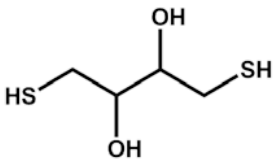

DTT (dithiothreitol)
MW 154

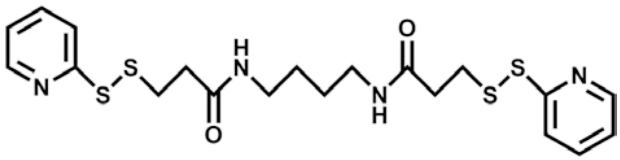

DPDPB (1,4-Di-[3´-(2´-pyridyldithio)-propionamido]butane)
MW 483

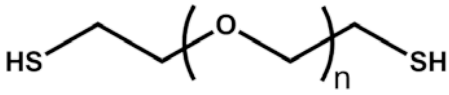

SH-PEG-SH (Polyethylene glycol dithiol)
MW 2000

Sup. Fig. 5

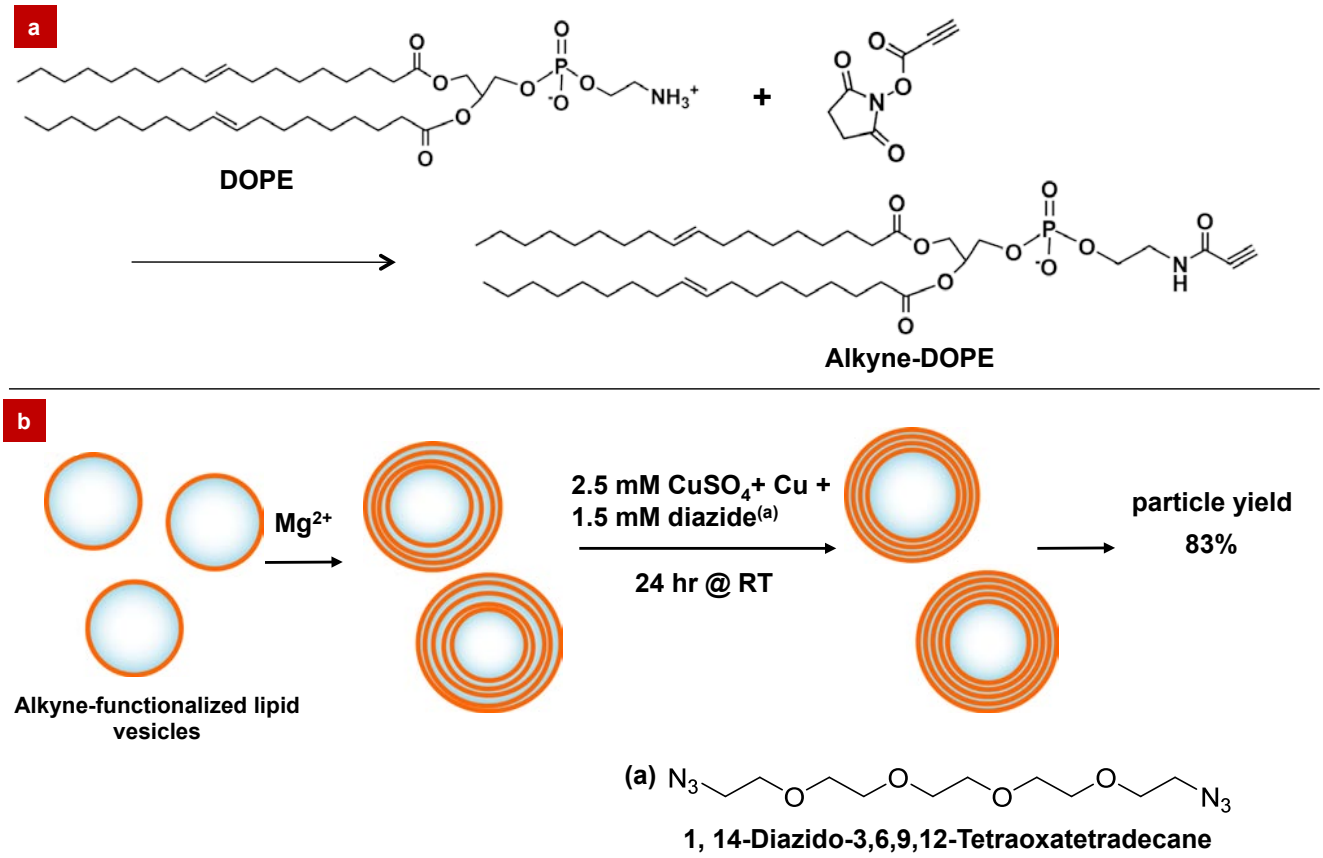

DOI: 10.1038/NMAT2960

Sup. Fig. 6

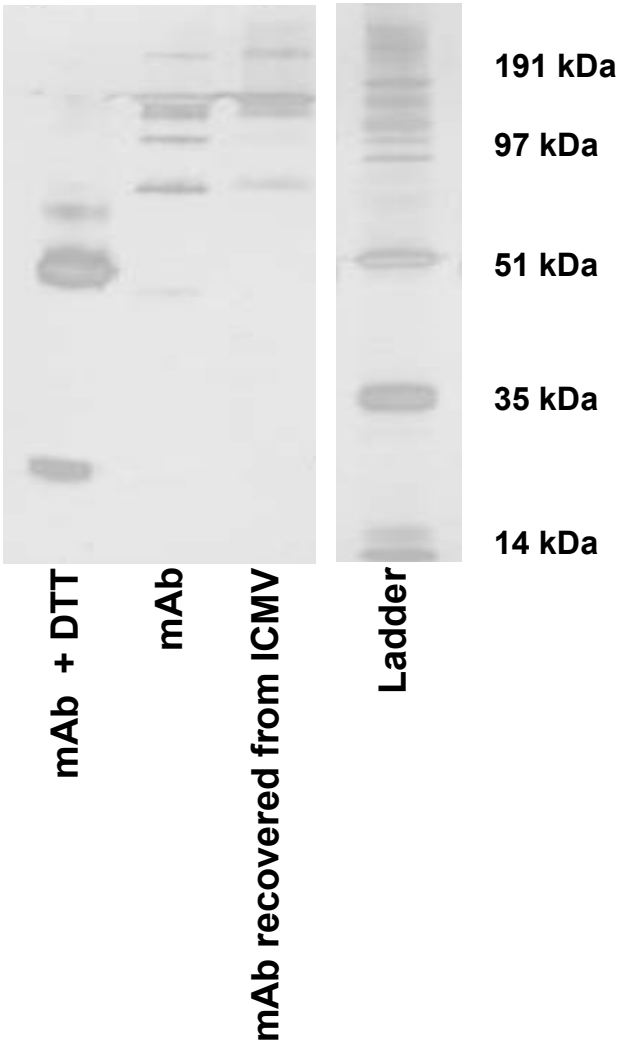

Sup. Fig. 7

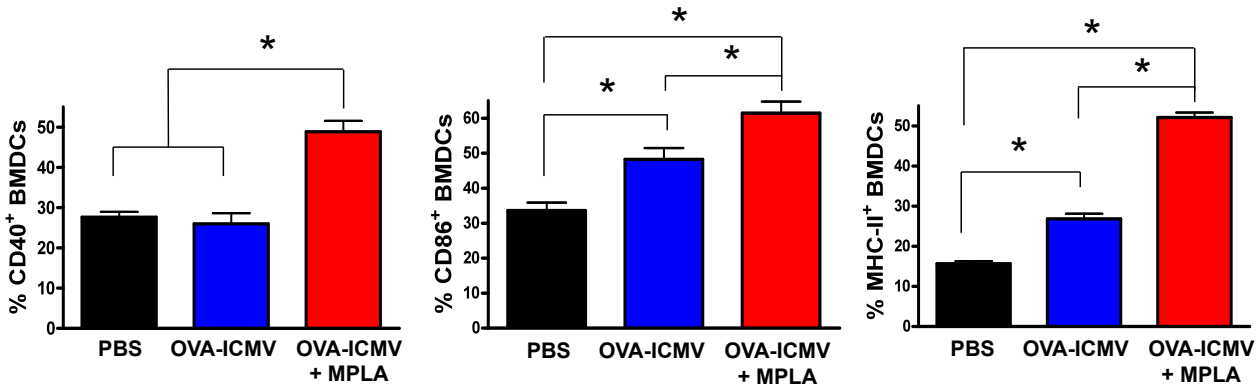

DOI: 10.1038/NMAT2960

Sup. Fig. 8